NMR Quantum Toys

JAE-SEUNG LEE, ANATOLY K. KHITRIN

Department of Chemistry, Kent State University, Kent, OH 44242-0001

ABSTRACT: Clusters of dipolar-coupled nuclear spins are excellent model systems for implementing various quantum experiments. The presented examples demonstrate recent techniques of coherent control for spin systems, as well as quantum dynamic schemes, like amplified quantum detection and measurement, state purification, adiabatic transfer of coherences, or projective measurement with NMR. Concepts Magn Reson Part A 30A: 194–217, 2007.

KEY WORDS: pseudopure states; quantum amplifier; amplified quantum measurement; quantum butterfly effect; quantum domino; resurrection of Schrödinger cat; projective measurement; adiabatic transfer of coherences

INTRODUCTION

There are several factors, which make clusters of coupled nuclear spins truly unique systems for experimental studies of quantum dynamics. Nuclear spin degrees of freedom can be extremely well isolated from the other degrees of freedom (lattice). In liquids and liquid crystals, fast molecular motions average out intermolecular spin–spin interactions and convert a system into an ensemble of noninteracting spin clusters. Liquid-crystalline solvents can be used to preserve anisotropic intramolecular interactions. Desired spin Hamiltonians can be created by choosing or synthesizing an appropriate molecule, and by specific isotope labeling. Therefore, one can prepare well-isolated spin clusters with desired and known spin Hamiltonians. Modern NMR spectrometers are specially designed to allow a precise coherent control over spin dynamics. Modulation with radiofrequency (RF) pulses can be sufficiently fast to convert the spin Hamiltonians into effective (average) Hamiltonians. This allows, as an example, studying quantum dynamics with Hamiltonians, which naturally do not exist.

Clusters of up to 12 spins ½, used in the experimental examples below, are still toys, in a sense that their quantum dynamics can be simulated using modern computers. However, they are, at present, the largest and the most complex quantum systems where individual quantum states have been addressed and coherently manipulated. They present an excellent test bed for trying new quantum algorithms and exploring unknown features of collective quantum dynamics.

This review highlights our results on implementing various schemes of quantum experiments using clusters of 6, 7, and 12 dipolar-coupled nuclear spins of (labeled) benzene in a liquid crystalline matrix. The paper is organized as follows. First, we describe the methods of preparing pseudopure states in clusters of homonuclear and heteronuclear dipolar-coupled spins. The technique is then extended to build the 12-spin "Schrödinger cat" state. Next, some algorithms exploiting the "cat" states are demonstrated on a 7-spin cluster: quantum amplifier, amplified measurement of quantum state, and "resurrection of Schrödinger cat." Finally, we demonstrate that NMR experiments can provide information about

Received 22 January 2007; revised 12 April 2007; accepted 24 April 2007

Correspondence to: J.-S. Lee; E-mail: jlee2@kent.edu

Concepts in Magnetic Resonance Part A, Vol. 30A(4) 194–217 (2007)

Published online in Wiley InterScience (www.interscience.wiley.com). DOI 10.1002/cmr.a.20084

possible outcomes of projective measurement and probabilities of such outcomes, and that the quantum coherences can be efficiently transferred via multiple adiabatic energy-level crossings.

PSEUDOPURE STATES

At thermal equilibrium, nuclear spin systems are in highly mixed states, which mean that individual system can be, with some probability, in any of many possible quantum states. The idea of state initialization by creating a so-called pseudopure state was originally proposed for NMR-based quantum computing (QC) (*1*, *2*). In a pseudopure state, populations of all but one state are made equal. As a result, the spin density matrix is a sum of a maximally mixed background, which is proportional to the identity matrix, and a deviation part, which is proportional to a density matrix of a pure state. The identity matrix does not contribute to observables and is not changed by unitary transformations. Therefore, the unitary dynamics of a system in a pseudopure state is exactly the same as it would be at zero spin temperature.

Pseudopure states have been used in NMR implementations of QC algorithms (*1–4*), quantum simulations (*5*, *6*), and demonstration of quantum mechanisms of amplified detection (*7*) and measurement (*8*). With conventional approaches using qubit-selective or transition-selective (*9*) pulses to equalize populations, there are two major limitations on the system's size: spectral resolution and the length of a pulse sequence. Both the number of allowed transitions and the length of the pulse sequence grow with the system's size. With multifrequency irradiation, it is possible to cause fast and efficient simultaneous evolution of all populations to desired values (*10*), but this technique also requires a well-resolved spectrum.

From a traditional NMR point of view, pseudopure states are nonequilibrium highly correlated states, which produce very unusual linear-response spectra. Let us consider the following simple example. Suppose that there are two spins with different Larmor frequencies and zz-interaction between them. There are four quantum states: $|\uparrow\uparrow\rangle$, $|\uparrow\downarrow\rangle$, $|\downarrow\uparrow\rangle$, and $|\downarrow\downarrow\rangle$, and four peaks in the thermal-equilibrium spectrum, corresponding to single-quantum (SQ) transitions between these states. The peak for each spin is split into two peaks by interaction with the neighbor spin. If a pseudopure state is prepared, where populations of the three states other than $|\uparrow\uparrow\rangle$ are equal, there remain only two peaks in the linear-response spectrum and only two frequencies in the corresponding free induction signal. Splitting caused by interaction with the neighbor spin disappears. Each spin is still up or down with almost equal probability, but the spectrum is the same, except for lower intensity, as for 100% polarized system, and the spins "feel" only one of the two possible local fields created by its neighbor. Therefore, pseudopure states can be used to simplify NMR spectra.

In this paper, the term "linear-response spectrum" is used frequently. It is defined as the imaginary part of magnetic susceptibility in the limit of zero amplitude of the excitation field. In a conventional Fourier-transform NMR, where the spectra are obtained by Fourier transforming the free induction decays, the spectra do not depend on the flip angle of the excitation pulse (except for their intensity) and coincide with the linear-response spectra. This is only true for high-temperature spin states with Zeeman order. In a general case, the spectrum depends on the flip angle of the excitation pulse. The linear-response spectra, that provide direct information about differences of populations, are Fourier transforms of the free induction signals, excited by a pulse with an infinitely small flip angle. In practice, we used small-angle reading pulses with flip angles between 1° and 10°. In each particular experiment, the choice was made by decreasing the flip angle until the spectrum stop changing.

Pseudopure States in Spin Clusters with Unresolved Spectra

In this section, we describe a method of creating pseudopure spin states in large clusters of coupled spins (*11*). It is based on filtering multiple-quantum (MQ) coherence of the highest order, followed by a time-reversal period and partial saturation. The first experimental example is a cluster of six dipolar-coupled proton spins of a benzene molecule in liquid crystalline matrix. It is a relatively small quantum system with $2^6 = 64$ states and well-resolved NMR spectrum. Later we will show how further development of this technique allows addressing individual quantum states in larger clusters with truly unresolved spectra.

The first step of many quantum algorithms is the state initialization or preparation of a pseudopure state (*1*, *2*). Conveniently, the algorithms start with a pseudopure ground state with equal populations of all states except the ground state. Algorithms, involving up to 7 and, more recently, 12 qubits have been realized with liquid-state NMR (*12*, *13*). Until now, all practical schemes used transition-selective or qubit-selective pulses for the state initialization. Therefore, the size of a spin system which can be prepared in a

pseudopure state has been limited by spectral resolution. For an N-spin system, the number of quantum levels 2^N grows very fast with increasing number of spins, and the number of peaks in NMR spectrum increases even faster. As an example, the maximum number of peaks for N dipolar-coupled spins is $\binom{2N}{N+1} \sim 2^{2N}$. The number of operations or the length of a pulse sequence needed for state preparation also grows with the number of spins.

In contrast to the thermal equilibrium state, which contains all quantum states, the highest-order multiple-quantum (HOMQ) coherence is built of only two states, $|u\rangle$ and $|d\rangle$, where $|u\rangle$ is the state with all spins up and $|d\rangle$ is the state with all spins down. The relation between the HOMQ coherence and the maximally entangled "Schrödinger cat" state $(|u\rangle + |d\rangle) \times (\langle u| + \langle d|)$ has been discussed in (*14*), where the implemented logic circuit used qubit-selective pulses and required a resolved spectrum. At the same time, there exist efficient techniques for exciting MQ coherences (*15–17*), which use sequences of nonselective hard pulses and can be applied to systems with unresolved spectra.

Our scheme consists of the following steps: excitation of MQ coherences (preparation period), filtering the HOMQ coherence, time-reversal period, and partial saturation. MQ coherences are excited by the multipulse sequence with an 8-pulse cycle (*15*), which creates the double-quantum (DQ) effective Hamiltonian

$$H_{\mathrm{av}} = H^{+2} + H^{-2} = -\frac{1}{2}\sum_{i<j} D_{ij}\left(I_{i+}I_{j+} + I_{i-}I_{j-}\right), \qquad [1]$$

where $I_{\pm} = I_x \pm iI_y$ and D_{ij}'s are the dipolar coupling constants. This effective Hamiltonian excites MQ coherences of all even orders. The HOMQ coherence can be excited in clusters of $2 + 4n$ ($n = 0, 1, 2, \ldots$) coupled spins. In finite clusters, intensities of individual MQ coherences oscillate. Total duration of the pulse sequence is adjusted to correspond to one of the maxima of HOMQ coherence. A combination of phase cycling and 180° pulse is used to average out all MQ coherences except the HOMQ coherence (*18*). The deviation density matrix after this temporal averaging is $i(|u\rangle\langle d| - |d\rangle\langle u|)$. Then the time-reversal period of the same duration follows. The pulse sequence for this period is the same as for the preparation period except that the phases of all pulses are shifted by 90°. This sequence creates the effective Hamiltonian $-H_{\mathrm{av}}$. After the time-reversal period, off-diagonal elements of the density matrix are small

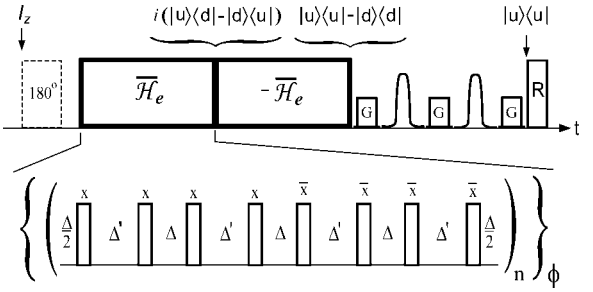

Figure 1 Scheme of the NMR pulse sequence for creating the pseudopure ground state.

if its duration corresponds to a maximum of the HOMQ intensity. Then, from conservation of $\mathrm{Tr}\{\rho\}$, $\mathrm{Tr}\{\rho^2\}$, and $\mathrm{Tr}\{\rho^2 H_{\mathrm{av}}^2\}$ during the unitary time-reversal period, we conclude that the deviation density matrix becomes $|u\rangle\langle u| - |d\rangle\langle d|$.

The state $|u\rangle\langle u| - |d\rangle\langle d|$ is a mixture of two states, which means that a nonunitary operation is needed to prepare the pseudopure ground state $|u\rangle\langle u|$. We used partial saturation, which redistributes the excessive population of the state $|d\rangle\langle d|$ among other states but does not change the population of the state $|u\rangle\langle u|$. If irradiation does not contain frequencies of transition from the ground state, the population of the ground state remains "trapped." In this experiment we used shaped Gaussian pulses for the partial saturation.

The physical system was six dipolar-coupled proton spins of a benzene molecule dissolved in liquid crystal ZLI 1167. Details of the sample preparation and parameters of the spin Hamiltonian are described elsewhere (*19*). The experiment has been performed with a Varian Unity/Inova 500 MHz NMR spectrometer. The pulse sequence for preparation of the pseudopure ground state $|u\rangle\langle u|$ is displayed in Fig. 1. Both of the shaped pulses had 1.5-ms duration and maximum amplitude $\gamma B_1/2\pi = 1.5$ kHz. The gradient pulses G are applied to assist eliminating the unwanted coherences. The pulse R is a small-angle reading pulse with a flip angle 5°.

The spectrum at thermal equilibrium is shown in Fig. 2(a). Positions and intensities of 76 peaks are determined by dipole–dipole interactions between six proton spins of the benzene molecule (*20*). The linear-response spectrum, corresponding to the state $|u\rangle\langle u| - |d\rangle\langle d|$ is presented in Fig. 2(b). The central frequency of the saturating Gaussian pulses was set to the frequency of SQ transition from the state $|d\rangle\langle d|$ [the left peak in Fig. 2(b)]. The spectrum of the saturating pulse covers mostly the left side of the spectrum while the intensity at the frequency of transition from the state $|u\rangle\langle u|$ [the right peak in Fig. 2(b)] is

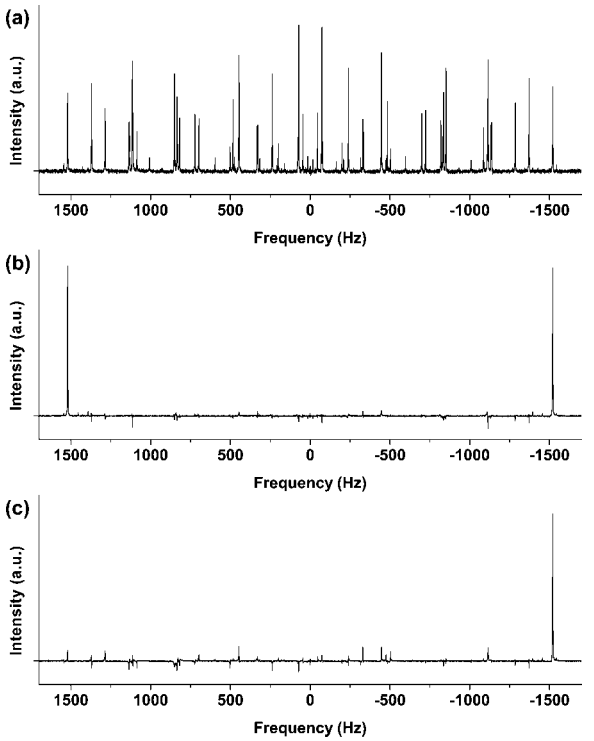

Figure 2 (a) Conventional ^{1}H NMR spectrum of benzene in liquid crystal; (b) linear-response spectrum for the state $|u\rangle\langle u|-|d\rangle\langle d|$; (c) linear-response spectrum for the pseudopure ground state $|u\rangle\langle u|$; Flip angle of the reading pulse was 5° for all spectra.

very small. As one can see in Fig. 2(c), population of the state $|u\rangle\langle u|$ is practically unaffected by the saturating pulses. The peak intensity is 5.5% of the integral intensity of the thermal equilibrium spectrum. The theoretical maximum (*21*) $N\times 2^{-N}$ is 9.3% for this system. It should be noted that the spectra in Figs. 2(b,c) are not MQ spectra but conventional SQ linear-response spectra for unusual and strongly correlated spin states.

For the pseudopure ground state of the N-spin cluster, there exist no more than N peaks in the linear-response spectrum. The spectrum can be well-resolved even for very large clusters of coupled spins. Starting with this simplified spectrum, it is possible to apply selective pulses for manipulating individual states and observing their dynamics. As an example, relaxation and decoherence rates of individual quantum states can be measured.

Pseudopure State of a Twelve-Spin System

The system described in this section is a cluster of dipolar-coupled nuclear spins of fully labeled $^{13}C_6$-benzene in a liquid crystalline matrix (*22*). It is a complex system of dipolar-coupled spins with $2^{12} = 4096$ quantum states.

The method is an extension of the technique used to prepare a pseudopure state in a cluster of seven dipolar-coupled nuclear spins: single-labeled ^{13}C-benzene in liquid-crystalline solvent (*8*). Here we apply a double-filtering using both phase cycling and an array of evolution times to create pseudopure states in a system consisting of two types of nuclear spins. The experiment has been performed with a Varian Unity/Inova 500 MHz NMR spectrometer. The sample contained 5% of fully labeled $^{13}C_6$-benzene (Aldrich) dissolved in liquid-crystalline solvent MLC-6815 (EMD Chemical).

The ^{1}H thermal equilibrium spectrum of $^{13}C_6$-benzene in MLC-6815 is shown in Fig. 3. It consists of a broad, about 20 kHz, spectrum of liquid crystal and, on top of its left slope, a poorly resolved spectrum of $^{13}C_6$-benzene with a width of about 5 kHz. The two sharp peaks in Fig. 3 are due to impurities. The proton signal from liquid crystal has been eliminated with a two-frequency saturation. According to the Provotorov's saturation theory (*23*), the off-resonance saturation results in a stationary state with nonzero Zeeman and dipolar temperatures. If saturation is performed at two different frequencies, the only stationary solution gives infinite spin temperature (zero magnetization). As a result, saturation at two frequencies outside the spectrum of $^{13}C_6$-benzene completely eliminates the signal of a liquid-crystalline matrix. The "purified" ^{1}H spectrum of $^{13}C_6$-benzene is presented in Fig. 5(a), which is a nice and symmetric spectrum with flat baseline. The impurity peak is marked with an asterisk.

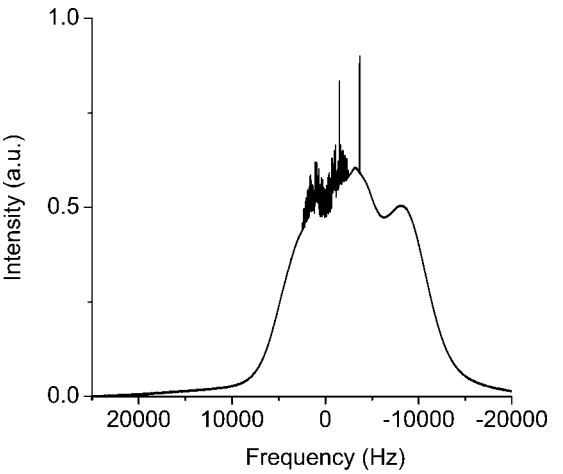

Figure 3 ^{1}H NMR spectrum of $^{13}C_6$-benzene in liquid crystal MLC-6815 at 25°C.

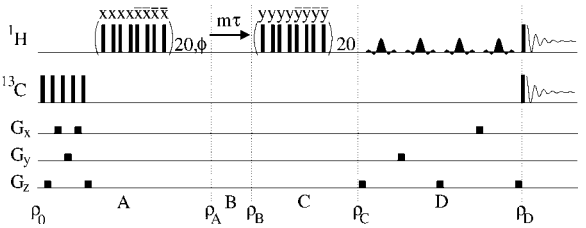

Figure 4 NMR pulse sequence for creating the 12-spin pseudopure state. For the notations, see the text.

For further discussion it will be convenient to use compact notations for spin states. The symbols $|u\rangle_H = |\uparrow\uparrow\uparrow\uparrow\uparrow\uparrow\rangle_H$ and $|d\rangle_H = |\downarrow\downarrow\downarrow\downarrow\downarrow\downarrow\rangle_H$ will denote the states of the proton spins with all six spins up and down, respectively. Similarly, the notations $|u\rangle_C$ and $|d\rangle_C$ will be used for the ^{13}C spin states with all six carbon spins up or down.

The experimental scheme is shown in Fig. 4.

Step A: It starts with a sequence of ^{13}C RF pulses and gradient pulses to saturate the ^{13}C magnetization, followed by the excitation of the MQ coherence and filtering of the HOMQ coherence, six-quantum (6Q) in this experiment, for proton spins. Twenty cycles of the 8-pulse sequence (*15*) for exciting proton spins' MQ coherence automatically decouple the carbon spins. The deviation density matrix after this first filtering becomes $\rho_A = 1_C \otimes i(\langle u\rangle\langle d| - \langle d\rangle\langle u|)_H$.

Step B: The secular dipole–dipole interactions between heteronuclei consist of *zz*-terms only. The *zz*-interaction with the ^{13}C spins causes a rotation of the proton spins' 6Q coherence, which does not evolve under the homonuclear dipole–dipole interactions between proton spins (*7*, *8*). The phase of this rotation is proportional to the evolution time τ and the total *z*-component of the ^{13}C spins. Similar to filtering the 6Q coherence using an array of phases, it is possible to filter out the two states of the ^{13}C spins with the extreme values of *z*-component of the total ^{13}C spin, which are ± 3, using an array of the evolution times $m\tau$ with $m = 0, 1, 2, \ldots$ The unit of the evolution time $\tau = 65.6$ μs corresponds to a rotation of the protons' 6Q coherence by π when the ^{13}C spins are in the state $|u\rangle_C$ or $|d\rangle_C$. After this second filtering, the deviation density matrix becomes $\rho_B = (|u\rangle\langle u| + |d\rangle\langle d|)_C \otimes i(|u\rangle\langle d| - |d\rangle\langle u|)_H$. The total number of experiments in this phase–time double array is only $12 \times 6 = 72$.

Step C: The second 20-cycle evolution period converts the proton spins' 6Q coherence into a diagonal state. This creates the density matrix $\rho_C = (|u\rangle\langle u| + |d\rangle\langle d|)_C \otimes (|u\rangle\langle u| - |d\rangle\langle d|)_H$ which is a mixture of the four pure states: $|u\rangle_C|u\rangle_H$, $|u\rangle_C|d\rangle_H$, $|d\rangle_C|u\rangle_H$, and $|d\rangle_C|d\rangle_H$. Due to the high symmetry of the system, there is only one ^{1}H or ^{13}C allowed SQ transition from each of these four states. The linear-response ^{1}H and ^{13}C spectra of the four-state mixture are shown in Figs. 5(b,b′), respectively.

Step D: A single pseudopure state has been selected by a partial saturation with four ^{1}H *sinc*-shaped pulses. The linear-response ^{1}H and ^{13}C spectra of the pseudopure state $|d\rangle_C|d\rangle_H$ are presented in Figs. 5(c,c′), respectively. Using the state $|d\rangle_C|d\rangle_H$ as an initial state, the other three states: $|u\rangle_C|u\rangle_H$, $|u\rangle_C|d\rangle_H$, and $|d\rangle_C|u\rangle_H$ can be obtained by applying nonselective "hard" π-pulses to ^{13}C and proton spins. One of the examples is shown in Figs. 5(d,d′), where ^{13}C π-pulse has been applied to the state $|d\rangle_C|d\rangle_H$ to create the state $|u\rangle_C|d\rangle_H$.

Twelve-Spin "Schrödinger Cat"

Here we demonstrate the pseudopure "cat" state, a superposition of quantum states with all spins up and all spins down for a system of 12 dipolar-coupled nuclear spins of fully ^{13}C-labeled benzene in a liquid-crystalline matrix (*24*).

Quantum entanglement, a form of nonclassical correlation, has been an important issue in recent debates on the foundations of quantum mechanics (*25*). In quantum information science, the entanglement is considered as a physical resource, which plays a crucial role in quantum teleportation (*26*), quantum key distribution (*27*, *28*), and QC (*29*, *30*). A cat state is a special case of entanglement: superposition of the two most distinct states (*alive* and *dead*). Building a cat state is a benchmark for controlling quantum systems (*14*). The decoherence time of the cat state sets limitation on QC because this state is supposed to be the most fragile among quantum states.

The experimental scheme is shown in Fig. 6. It consists of the three parts: preparation of the pseudopure state as described above (step A), creation of the 12-spin cat state (steps B–E), and its verification and life-time estimation (steps F–J). The pulse sequence in step A initializes our system in a pseudopure state $|\Psi_A\rangle = |d\rangle_C|d\rangle_H$. The ^{1}H linear-response spectrum of $|\Psi_A\rangle$ is presented in Fig. 7(a). Hard pulses (180°) on both protons and carbons convert the state $|\Psi_A\rangle$ into the pseudopure state $|u\rangle_C|u\rangle_H$ [Fig. 7(b)].

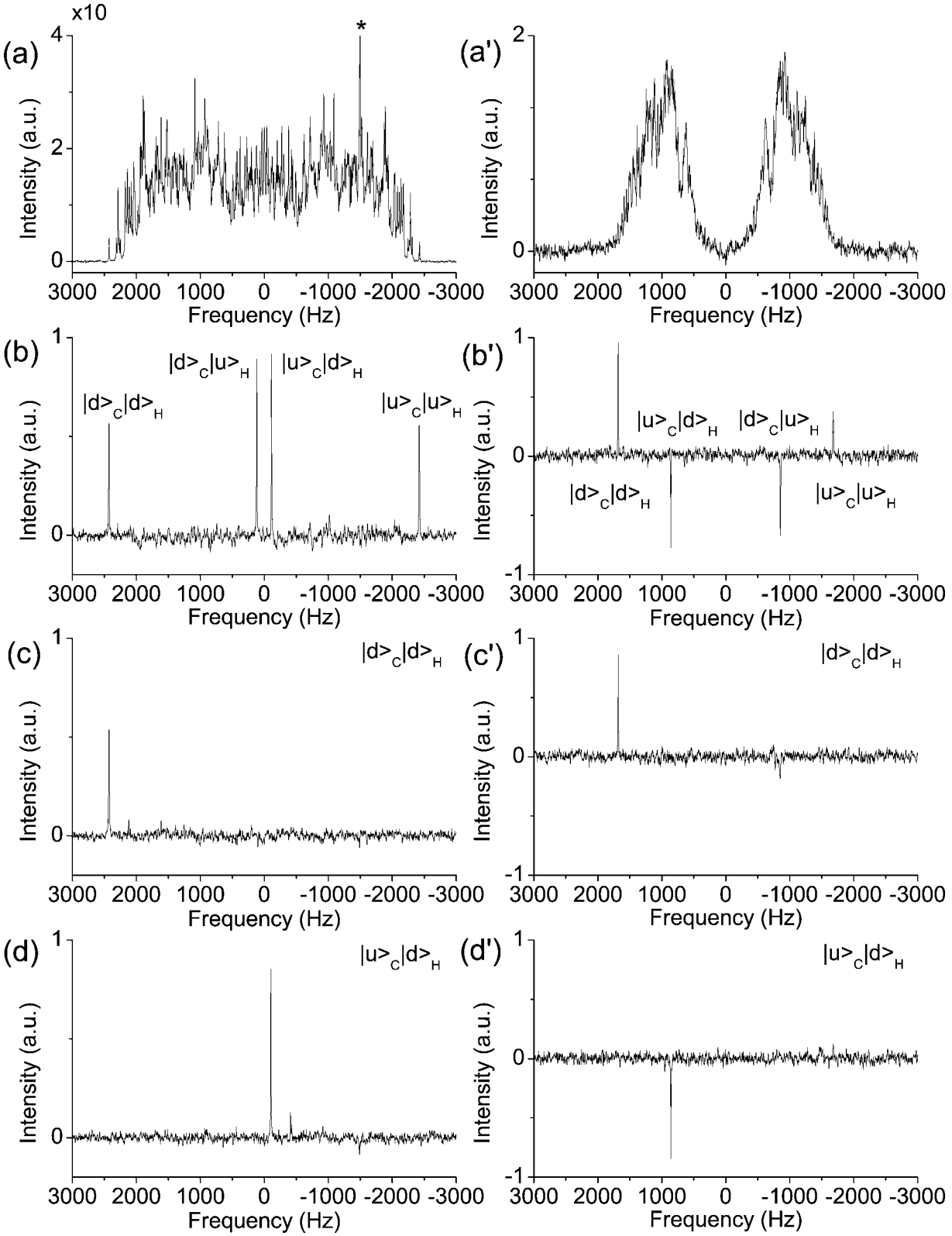

Figure 5 (a) ^{1}H and (a′) ^{13}C NMR spectra of the thermal equilibrium state; (b) ^{1}H and (b′) ^{13}C spectra of the mixture of four states: $\rho_C = (|u\rangle\langle u| + |d\rangle\langle d|)_C \otimes (|u\rangle\langle u| - |d\rangle\langle d|)_H$; (c) ^{1}H and (c′) ^{13}C spectra of the pseudopure state $|d\rangle_C|d\rangle_H$; (d) ^{1}H and (d′) ^{13}C spectra of the pseudopure state $|u\rangle_C|d\rangle_H$.

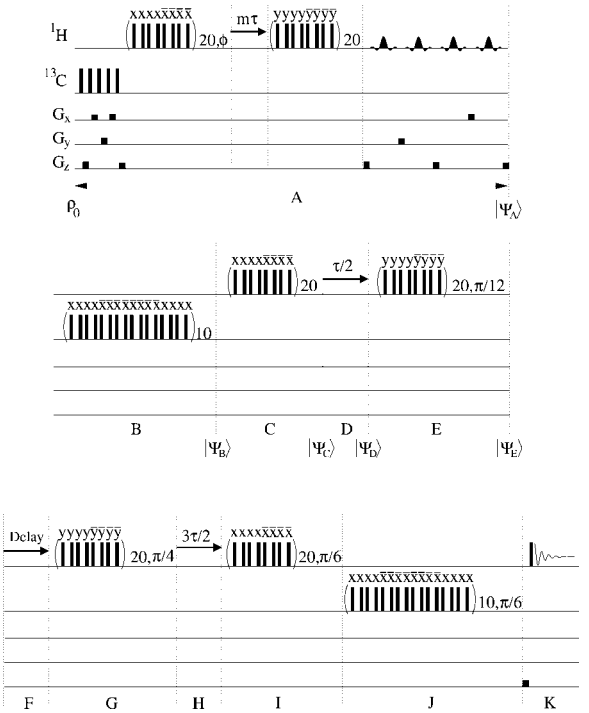

Figure 6 NMR pulse sequence for building a twelve-spin cat state. For ^{1}H and ^{13}C channels, rectangular and *sinc* shapes represent 90° hard and *sinc*-shaped pulses, respectively. The symbols x, y, $\bar{x}$, and $\bar{y}$ over the pulses represent relative phases or the directions of the pulses in the rotating frame. Pulsed gradient channels G_x, G_y, and G_z provide linear gradients of static magnetic field along the x, y, and z axes, respectively. (Step A) preparation of the pseudopure state; (steps B–E) creation of the 12-spin cat state; (steps F–J) state verification and life-time estimation.

In step B, 10 cycles of a 16-pulse sequence were applied to convert the state $|d\rangle_C$ into a superposition of $|u\rangle_C$ and $|d\rangle_C$. The 16-pulse sequence (*31*), with slightly better performance for ^{13}C spins, evolves the system with the same DQ Hamiltonian as the 8-pulse sequence (*15*) used for the proton spins. Therefore, with optimized parameters, the 16-pulse sequence transforms $|\Psi_A\rangle$ into $|\Psi_B\rangle = 2^{-1/2}(|u\rangle_C+|d\rangle_C)|d\rangle_H$. In step C, the 8-pulse sequence brings the proton spins into a superposition, and the state becomes $|\Psi_C\rangle = 2^{-1}(|u\rangle_C+|d\rangle_C)(|u\rangle_H+|d\rangle_H)$. In step D, free evolution gives phase factors according to a sum of the total z-components of proton and carbon spins: $|\Psi_D\rangle = 2^{-1}(|u\rangle_C|u\rangle_H-i|u\rangle_C|d\rangle_H-i|d\rangle_C|u\rangle_H+|d\rangle_C|d\rangle_H)$. Finally in step E, the 8-pulse sequence converts $|\Psi_D\rangle$ into the cat state $|\Psi_E\rangle = 2^{-1/2}\times(|u\rangle_C|u\rangle_H+|d\rangle_C|d\rangle_H)$. The spectrum for this state, shown in Fig. 7(c), is consistent with the equally-weighted superposition of $|u\rangle_C|u\rangle_H$ and $|d\rangle_C|d\rangle_H$. However, the linear-response spectrum depends only on the two diagonal elements of the corresponding density matrix. The other two off-diagonal elements of the cat state density matrix constitute the 12-quantum coherence, which is not directly observable.

Therefore, we added the state-verification steps by time-reversing the sequences of the steps B–E. The pulse sequences and their phases were arranged so that steps G, H, I, and J are respectively the inverses of the steps E, D, C, and B. The delay step F was added for measuring decoherence time of the cat state. With no delay in step F, we expected that the state would be converted back to the state $|\Psi_A\rangle$. Figure 7(d) shows the result of such experiment. It confirms that the state $|\Psi_E\rangle$ after the step E is a superposition of the states $|u\rangle_C|u\rangle_H$ and $|d\rangle_C|d\rangle_H$ rather than their mixture.

QUANTUM AMPLIFIER

With nonlinear classical dynamics, two states of a system, which are close at one moment of time, can

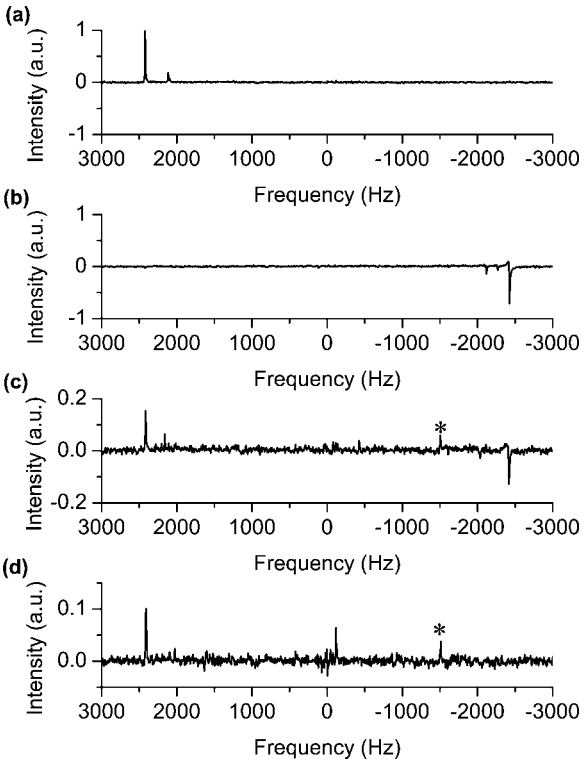

Figure 7 ^{1}H NMR linear-response spectra: (a) pseudopure state $|d\rangle_C|d\rangle_H$; (b) pseudopure state $|u\rangle_C|u\rangle_H$ obtained from $|d\rangle_C|d\rangle_H$ by applying 180° hard pulses to both proton and ^{13}C spins; (c) a cat state, superposition of $|d\rangle_C|d\rangle_H$ and $|u\rangle_C|u\rangle_H$; (d) $|d\rangle_C|d\rangle_H$ after the time-reversed sequences of entangling operations.

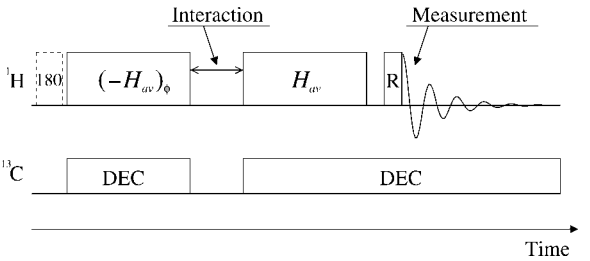

Figure 8 Scheme of the NMR pulse sequence for quantum amplifier.

exponentially diverge at later time. Such evolution may amplify small perturbations and result in the so-called "butterfly effect" (*32*). This property of nonlinear dynamics can be beneficial in measuring small signals. On the other hand, quantum dynamics is governed by linear equations of motion. Unitary evolution operators conserve distances between states: the states that are close at one moment of time remain close at all times. This means that the classical mechanisms of amplifying weak signals cannot be implemented in quantum systems. However, quantum mechanics offers another alternative of converting a small perturbation into a big change in observable values. It is based on using special entangled states of a composite quantum system (*7*, *33*). For such states, perturbation acting on a small part of a system changes a state of the whole system in a coherent way and produces changes of "macroscopic" observables.

The experimental demonstration has been made using a system of seven dipolar-coupled nuclear spins of single-labeled ^{13}C-benzene molecules in a liquid-crystalline matrix.

The experimental scheme is shown in Fig. 8. Two evolution periods with the effective Hamiltonians of opposite signs constitute a time-reversal sequence. The ^{13}C spin is decoupled all the time except for a short perturbation period between the two evolution periods. The DQ effective Hamiltonian [1] is created by 20 cycles of the 8-pulse sequence (*15*). The HOMQ (6Q) coherence was filtered by a combination of phase cycling and 180° pulse. The first evolution period with 6Q filtering converts the initial thermal equilibrium state of proton spins into the state with the deviation density matrix $i(|u\rangle\langle d| - |d\rangle\langle u|)$. This matrix with two elements is the off-diagonal part of the "cat" state $(|u\rangle + |d\rangle)(\langle u| + \langle d|)$. The second, time-reversed, evolution period converts this state into the diagonal state with only two nonzero elements $|u\rangle\langle u| - |d\rangle\langle d|$. The sample contained 5% of single-labeled ^{13}C-benzene (Aldrich) dissolved in liquid-crystalline solvent MLC-6815 (EMD Chemical).

The ^{1}H thermal equilibrium spectrum of ^{13}C-benzene in MLC-6815 without ^{13}C decoupling is shown in Fig. 9(a). The proton spectrum with ^{13}C decoupling is shown in Fig. 9(b). The peaks are somewhat broader in the ^{13}C-decoupled spectrum due to nonperfect decoupling and RF heating of the sample. We have found that CW decoupling is not very efficient and that the two-pulse phase-modulation (TPPM) decoupling sequence (*34*) with the phase excursion angle 54° gave better results and was used in the experiment. The RF power level was a compromise between the decoupling quality and the RF heating, which creates temperature gradients and broadens the peaks. The rightmost peak in Fig. 9(b) is due to impurity.

A linear-response spectrum corresponding to the state $|u\rangle\langle u| - |d\rangle\langle d|$ is presented in Fig. 9(c). Due to the high symmetry of a benzene molecule, there is only one allowed SQ transition from each of the states: all spins up and all spins down. The two peaks in spectrum 9(c) are at the frequencies of these tran-

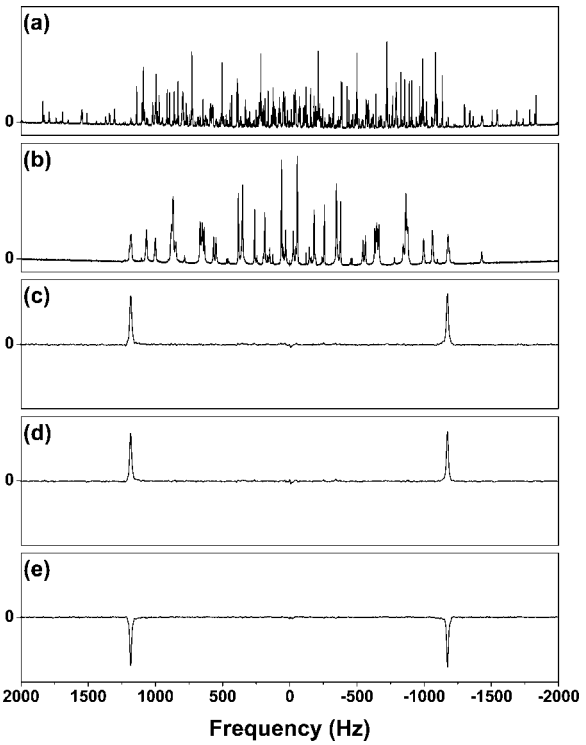

Figure 9 (a) ^{1}H thermal equilibrium spectrum of ^{13}C-benzene in MLC-6815; (b) 1H spectrum with ^{13}C decoupling; (c) linear-response spectrum after the time-reversal sequence with 6Q filtering (^{13}C spin decoupled); (d) spectrum with the delay of 382.5 μs (perturbation period) in between the two evolution periods (^{13}C spin decoupled); (e) spectrum with the decoupling turned off during the perturbation period.

sitions. When 382.5-μs delay was introduced between the two evolution periods and the ^{13}C spin was decoupled during this perturbation period, there were no noticeable changes in the spectrum [Fig. 9(d)]. However, if the decoupling was off, the spectrum reversed, indicating that the magnetization of proton spins changed its sign [Fig. 9(e)].

The mechanism of this magnetization reversal is the following. The 6Q deviation density matrix ρ_{6Q} after the first evolution period can be written, without a concern for a phase factor, as

$$\rho_{6Q} = S_1^+ S_2^+ S_3^+ S_4^+ S_5^+ S_6^+ + S_1^- S_2^- S_3^- S_4^- S_5^- S_6^-, \qquad [2]$$

where S_j^+ (S_j^-) are the raising (lowering) operators for the jth proton spin. The rotation of any one of the spins by the angle φ around z-axis adds only a phase factor to each of the two product terms of the density matrix [2] according to the relation $\exp(-i\varphi S_j^z)S_j^\pm \times \exp(i\varphi S_j^z) = S_j^\pm \exp(\mp i\varphi)$. Therefore, the result does not depend on whether all the spins are rotated by the same angle φ/6 or only one spin is rotated by the angle φ. As an example, when one of the spins is rotated by π the whole density matrix [2] changes its sign. As a result, the deviation density matrix after the second evolution period changes its sign and all observables, including the protons' magnetization, also change their signs. In our experiment such rotation was performed by interaction with the ^{13}C spin. The interaction between ^{13}C and the nearest proton (2035 Hz), which includes the dipole–dipole interaction (1877 Hz) and J-coupling (158 Hz), amounts to 80% of the ^{13}C–protons interaction (2549 Hz). During the 382.5-μs perturbation period, the spin of the proton nearest to ^{13}C is rotated by almost π, while the phases acquired by other proton spins remain small. However, the entangled state [2] is not "spoiled" by these inhomogeneous rotations, as if all the spins performed a coherent rotation. An interesting implementation of a coherent rotation of all spins in an entangled state is a high-precision spectroscopy, which can reach the Heisenberg limit (*35*). It should be noted that the experiment described here was not designed to measure the state of the ^{13}C spin.

The experiment showed a big change in observable values originating from perturbation acting on a small part of a quantum system, which looks similar to the classical "butterfly effect." The scheme of the time-reversal experiment in Fig. 8 follows a scenario of the story (*36*) where a small perturbation performed in the past produces dramatic changes in the present. The scenario can be implemented both with a classical dynamics and also with a quantum evolution, as it is demonstrated here. In contrast to a classical version, in a quantum experiment, big change of the state occurs "instantly" during the perturbation period. However, this change cannot be observed directly. A long evolution period is needed for correlations to propagate through the entire system and to convert a change of the state into a change of observable values.

AMPLIFIED MEASUREMENT OF QUANTUM STATE

Here we experimentally demonstrate that an arbitrary quantum state of a single spin ½: $a|\uparrow\rangle+b|\downarrow\rangle$ can be converted into a superposition of the two ferromagnetic states of a spin cluster: $a|\uparrow\uparrow\cdots\uparrow\uparrow\rangle+b|\downarrow\downarrow\cdots\downarrow\downarrow\rangle$ (*8*). The physical system is a cluster of seven dipolar-coupled nuclear spins of single-labeled ^{13}C-benzene molecules in a liquid-crystalline matrix.

Theory of quantum measurements, which describes a boundary between quantum and classical worlds (*37*, *38*), is the least established part of quantum theory. Different approaches to this problem lead to different interpretations of quantum mechanics (*39*). General aspects of measurements on ensembles have been discussed in recent paper (*40*). A serious difficulty in exploring this subject is that practical measuring devices are too complex to allow a detail analysis of their dynamics. It is helpful to consider some simple and explicit models of quantum measurement, using systems with controllable quantum dynamics.

Let us consider a system of $N + 1$ spins ½ (qubits) in the initial state

$$|\psi_{in}\rangle = \big(a|0\rangle_0+b|1\rangle_0\big)|0\rangle_1|0\rangle_2\cdots|0\rangle_{N-1}|0\rangle_N, \qquad |a|^2+|b|^2=1, \qquad [3]$$

where the qubit notations $|0\rangle_k \equiv |\uparrow\rangle_k$ and $|1\rangle_k \equiv |\downarrow\rangle_k$ are used. In this state, the 0th qubit is in some arbitrary state, defined by two complex coefficients a and b, while the qubits 1 to N are in the ground state. A quantum logic circuit (*8*, *41*) (a similar circuit has been proposed in (*33*))

$$U = \mathrm{CNOT}_{N-1,N}\mathrm{CNOT}_{N-2,N-1}\cdots\mathrm{CNOT}_{1,2}\mathrm{CNOT}_{0,1} \qquad [4]$$

is a chain of unitary controlled-not gates $\mathrm{CNOT}_{m,n}$, which flip the target qubit n when the control qubit m is in the state $|1\rangle_m$ and do not change the qubit n when the qubit m is in the state $|0\rangle_m$. If the 0th qubit is in the state $|1\rangle_0$, it flips the qubit 1, the qubit 1 flips

the qubit 2, and so on. A wave of flipped qubits, triggered by the 0th qubit, propagates until it covers the entire system. As a result, the circuit [4] converts the initial state [3] into the final state

$$|\psi_{\text{out}}\rangle = U|\psi_{\text{in}}\rangle = a|0\rangle_0|0\rangle_1\cdots|0\rangle_{N-1}|0\rangle_N + b|1\rangle_0|1\rangle_1\cdots|1\rangle_{N-1}|1\rangle_N. \quad [5]$$

This state is a superposition of the most macroscopically distinct states: the ferromagnetic states with all spins up and all spins down. It is interesting that there exists an analytically solvable model (*41*) with a "quantum domino" dynamics, similar to the dynamics suggested by the circuit [4].

One might think that, since a macroscopic polarization is associated with the state [5], a single measurement can provide some information about the state. However, transforming the state [3] to the state [5] does not decrease relative quantum fluctuations. As an example, an ensemble average of the square of polarization has its maximum value, $(N+1)^2$, which indicates that the possible outcomes of polarization measurement for a single system will be one of the two extreme values, $\pm(N+1)$. Therefore, the only goal of creating the state [5] is to increase a signal produced by a system, without making this signal more classical.

The experiment has been performed with a Varian Unity/Inova 500 MHz NMR spectrometer. The system is the same 7-spin cluster of singly labeled benzene. The spin Hamiltonian is

$$H = -\omega_C I_{0Z} - \omega_H \sum_{k=1}^{6} S_{kZ} + \sum_{k=1}^{6}(b_{0k} + J_{0k}) I_{0Z} S_{kZ} + \sum_{k>j>0}^{6} b_{jk}\left(S_{kZ}S_{jZ} - \tfrac{1}{2}S_{kX}S_{jX} - \tfrac{1}{2}S_{kY}S_{jY}\right), \quad [6]$$

where index 0 is used for the ^{13}C spin and indexes 1–6 numerate the proton spins, starting from the one closest to ^{13}C nucleus. I and S are corresponding spin operators, ω_C and ω_H are the Larmor frequencies, b_{jk} are the constants of residual dipole–dipole interaction, and J_{jk} are the J-coupling constants. Among J-constants, only J_{01} has a considerable value of $J_{01}/2\pi = 158$ Hz (*19*), the rest of the J-coupling constants are small and can be neglected on the time scale of our experiment. The ^{1}H and ^{13}C thermal equilibrium spectra of ^{13}C-benzene in MLC-6815 are presented in Figs. 11(a,a′), respectively. In what follows, we will use spin notations $|\uparrow\rangle$ and $|\downarrow\rangle$ for the two states of the ^{13}C spin, $|u\rangle = |\uparrow\uparrow\uparrow\uparrow\uparrow\uparrow\rangle$ and $|d\rangle = |\downarrow\downarrow\downarrow\downarrow\downarrow\downarrow\rangle$ for the states of proton spins with all spins up or down.

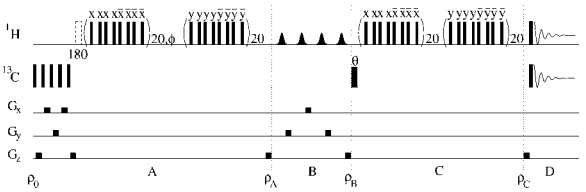

Figure 10 NMR pulse sequence for amplified measurement of quantum state.

As it was shown above, the superposition state of proton spins $2^{-1/2}(|u\rangle + |d\rangle)$ could be used to amplify the effect of interaction with ^{13}C spin (*7*). Some basic elements used in that experiment, together with preparation of the pseudopure state $|u\rangle$ for the proton subsystem (*11*), are also the building blocks of the experimental scheme in Fig. 10. To better understand the following steps, it is convenient to introduce the Pauli operators for a subspace of two proton states $|u\rangle$ and $|d\rangle$: $\Sigma_Z = |u\rangle\langle u| - |d\rangle\langle d|$, $\Sigma_X = |u\rangle\langle d| + |d\rangle\langle u|$, and $\Sigma_Y = i(|u\rangle\langle d| - |d\rangle\langle u|)$.

The first two steps, A and B (Fig. 10) are designed to prepare the pseudopure ground state $|\uparrow\rangle|u\rangle$ of the seven-spin cluster. Step A starts with a sequence of 90° pulses and gradient pulses to saturate the ^{13}C magnetization. Then, the proton magnetization is converted into MQ coherences by 20 cycles of the 8-pulse sequence (*15*), which automatically decouples protons from the ^{13}C spin, and the 6Q coherence Σ_Y is filtered. The next step is the evolution caused by the interaction with the ^{13}C spin, which rotates Σ_Y towards $\pm\Sigma_X$ depending on the state of the ^{13}C spin. After 90° rotation, the state density matrix $-I_{0Z}\Sigma_X$ is achieved. Then, evolution with another 20-cycle pulse sequence follows. The multipulse period, with about 90% fidelity, corresponds to a "90° pulse" in the Σ-subspace around some axis in the XY-plane. The phase of this "pulse" in the Σ-subspace is adjusted by the global phase of the pulse sequence. As an example, 90° phase shift can be achieved by $90°/6 = 15°$ phase shifting of all pulses of the sequence. The "90° Y-pulse" in the Σ-subspace converts the state $-I_{0Z}\Sigma_X$ into the state $\rho_A = I_{0Z}\Sigma_Z = (|\uparrow\rangle\langle\uparrow| - |\downarrow\rangle\langle\downarrow|)(|u\rangle\langle u| - |d\rangle\langle d|)$. This state is the mixture of four pseudopure states. The ^{1}H and ^{13}C linear-response spectra for this state are shown in Figs. 11(b,b′), respectively.

In step B, the pseudopure ground state $|\uparrow\rangle|u\rangle$ ($\rho_B = |\uparrow\rangle\langle\uparrow||u\rangle\langle u|$) is obtained by redistributing the excess population of the other three states by partial saturation. The ^{1}H and ^{13}C linear-response spectra for the pseudopure state $|\uparrow\rangle|u\rangle$ are presented in Figs. 11(c,c′), respectively. To verify the state, we applied

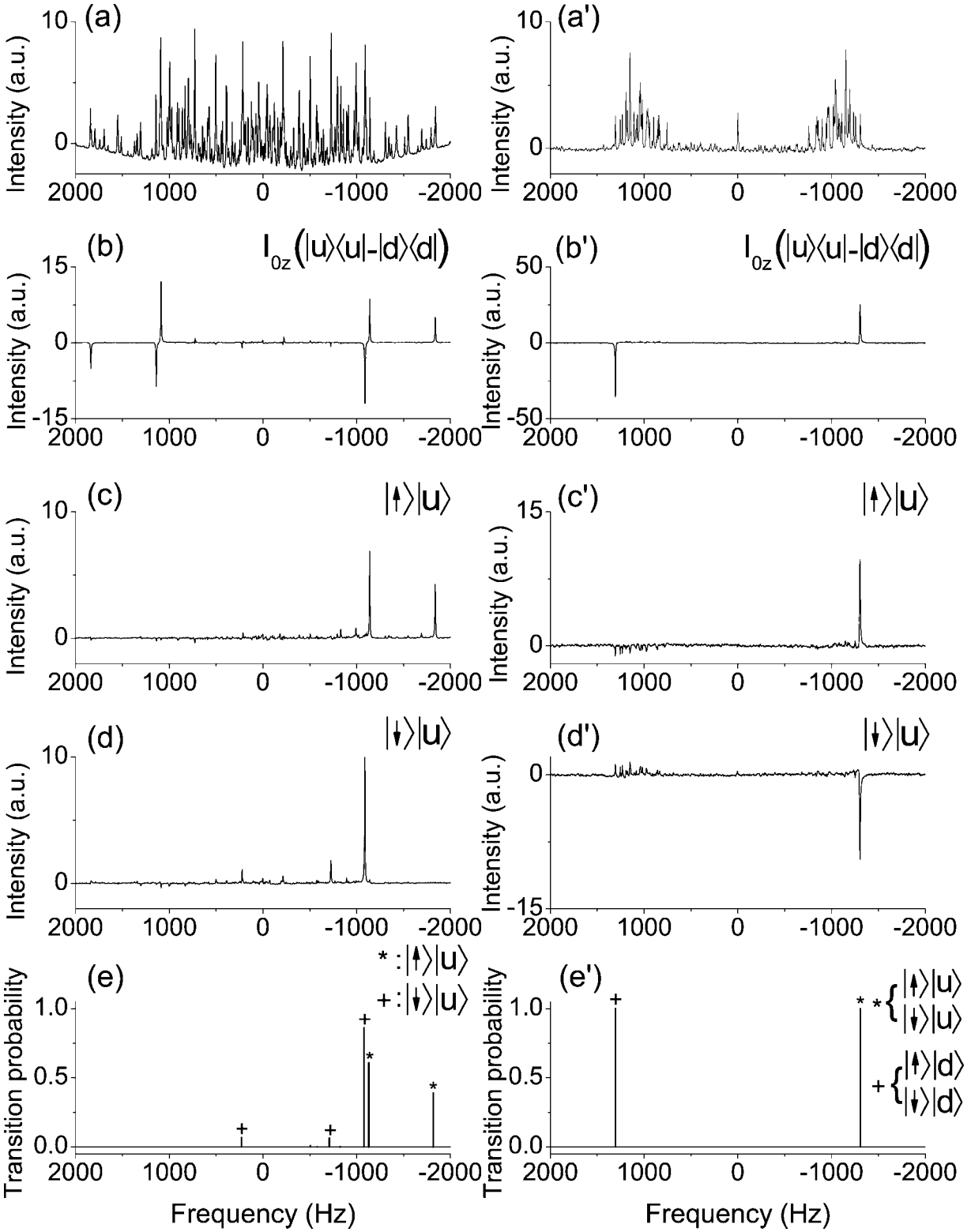

Figure 11 (a) ^{1}H and (a′) ^{13}C spectra of the thermal equilibrium state; (b) ^{1}H and (b′) ^{13}C spectra of the state $\rho_A = I_{0Z}\Sigma_Z$; (c) ^{1}H and (c′) ^{13}C spectra of the pseudopure state $|\uparrow\rangle|u\rangle$; (d) ^{1}H and (d′) ^{13}C spectra of the pseudopure state $|\downarrow\rangle|u\rangle$; numerically calculated (e) ^{1}H and (e′) ^{13}C spectra.

hard 180° pulses on the ^{13}C and proton spins and compared the spectra with numerically calculated spectra. As one illustration, the spectra for the state $|\downarrow\rangle|u\rangle$ are shown in Figs. 11(d,d′). The calculated spectra for the states $|\uparrow\rangle|u\rangle$ and $|\downarrow\rangle|u\rangle$ are shown in Figs. 11(e,e′).

In step C, a θ-pulse on the ^{13}C spin prepares the state [3] with $a = \cos(\theta/2)$ and $b = \sin(\theta/2)$. To convert this state into the state [5], the same pulse sequence as in step A was used without any phase cycling. The first "90° pulse" in the Σ-subspace converted the state of proton spins $|u\rangle$ to the entangled state $2^{-1/2}(|u\rangle + |d\rangle)$. Then, interaction delay caused Z-rotation in Σ-subspace, depending on the state of the ^{13}C spin, to yield the state $\cos(\theta/2)|\uparrow\rangle(|u\rangle + |d\rangle) + \sin(\theta/2)|\downarrow\rangle(|u\rangle - |d\rangle)$. The relative phase of the last 20-cycle pulse sequence was set to 45°, creating 270° phase shift in the Σ-subspace. This "90° pulse" in the Σ-subspace created the final state [5]: $\cos(\theta/2)|\uparrow\rangle|u\rangle + \sin(\theta/2)|\downarrow\rangle|d\rangle$. The linear-response spectra for this state at $\theta = 0°$, 90°, and 180° are shown in Fig. 12.

When the ^{13}C spin was prepared in an eigenstate $|\uparrow\rangle$ ($|\downarrow\rangle$), the 7-spin system resulted in the state with all spins up (all spins down) to give spectra of Figs. 12(a,a′) [Figs. 12(c,c′)]. When the ^{13}C spin was prepared in a superposition state $2^{-1/2}(|\uparrow\rangle + |\downarrow\rangle)$, the spectra in Figs. 12(b,b′) revealed proper correlation between the six proton and ^{13}C spins.

The implemented experimental scheme is an explicit model of quantum measurement. Six proton spins represent a measuring device designed to measure a quantum state of the ^{13}C spin. Conversion of the state [3] to the state [5] takes 7.2 ms. For our small system, this time is considerably shorter than the decoherence time, about 50 ms, of the seven-quantum (7Q) coherence in the state [5]. After a time, longer than the 7Q decoherence time but much shorter than T_1 (2 s), two off-diagonal elements of the density matrix of the state [5] decay, and the system reaches a mixed state with the density matrix $|a|^2|\uparrow\rangle\langle\uparrow||u\rangle\langle u| + |b|^2|\downarrow\rangle\langle\downarrow||d\rangle\langle d|$. This state is indistinguishable from the mixture, with fractions $|a|^2$ and $|b|^2$, of molecules in one of the two pure states: $|\uparrow\rangle|u\rangle$ or $|\downarrow\rangle|d\rangle$. Each of the molecules presents a result of individual measurement, where "macroscopic" magnetization of protons gives the result of this measurement while the state of the ^{13}C spin is collapsed to the corresponding eigenstate.

RESURRECTION OF SCHRÖDINGER CAT

Here we demonstrate that quantum state, destroyed by uncontrollable natural decoherence, can be purified by using results of projective measurement and converted into a desired target pure state. Physical system is a cluster of seven dipolar-coupled nuclear spins of single-labeled ^{13}C-benzene in liquid crystal. ^{13}C spin plays a role of a device for measuring protons' "cat" state, a superposition of states with six spins up (*alive*) and six spins down (*dead*). Information about the state, stored in the ^{13}C spin, is used to bring the protons' subsystem into the target *alive* state, while the excess entropy produced by decoherence is transferred to the "measuring device," the ^{13}C spin (*42*). Compared to the previous section, now a small subsystem (a single ^{13}C spin) plays a role of the measuring device.

Relaxation and decoherence, caused by interaction with environment, convert a pure quantum state of a system into a mixed one. The corresponding increase of entropy quantifies irreversibility and loss of information about the state. Projective measurement collapses the wave function into one of the known states and the result of measurement provides complete information about the system's state. Therefore, unitary transformations conditioned by the results of projective measurement can be used to assemble a desired pure state of the system.

The most striking difference between quantum and classical systems is the ability of quantum objects to be in a superposition state. A system in a superposition of macroscopically distinct states (*alive* and *dead* states of the "Schrödinger cat") would demonstrate highly unusual behavior. Recent proposals suggest that the cat state can play an important role in quantum-enhanced measurements: high-precision spectroscopy (*35*), amplified detection (*7*, *33*), and quantum state measurement (*8*). Decoherence resulting from interaction with environment is the major obstacle in designing practical devices.

When each of an ensemble of identical systems is characterized by the same quantum state, such an ensemble is said to be in a pure state and can be described by a wave function $|\Psi\rangle$ or, equivalently, by the corresponding density matrix $\rho = |\Psi\rangle\langle\Psi|$. When a system is in one of the two states: $|u\rangle$ (*alive*) or $|d\rangle$ (*dead*), in a basis where $|u\rangle$ and $|d\rangle$ are eigenstates, the density matrix has only one nonzero matrix element. For the superposition state $2^{-1/2}(|u\rangle + |d\rangle)$, the density matrix of this pure state contains four nonzero elements in the same basis. Two diagonal elements are the populations and the two off-diagonal elements describe a coherence between the two states. Interaction with environment can destroy the coherence. The result of this process, called decoherence, is the mixed state of an ensemble. Individual systems are no

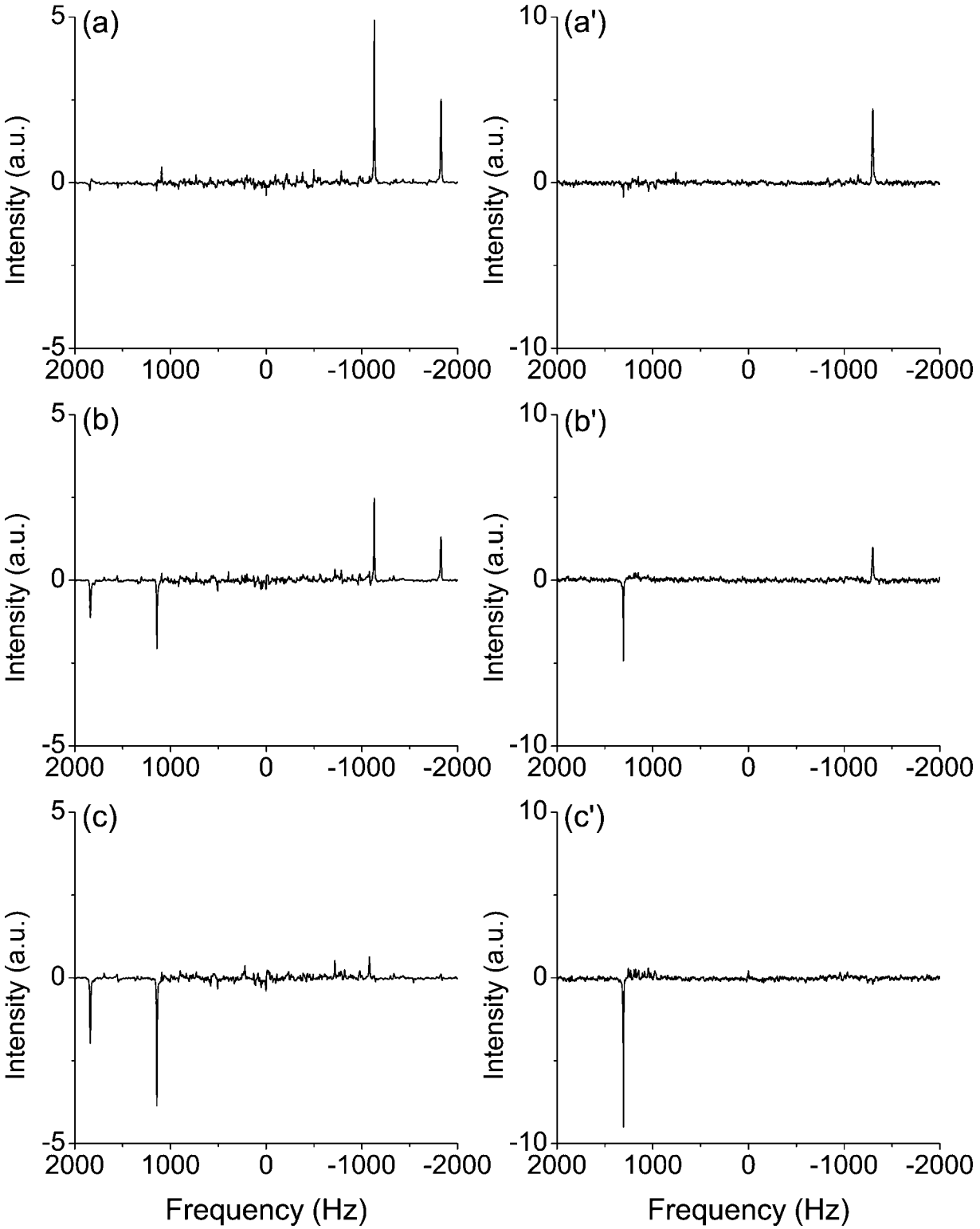

Figure 12 (a) and (a′) ^{1}H and ^{13}C spectra at $\theta = 0^{\circ}$; (b) and (b′) ^{1}H and ^{13}C spectra at $\theta = 90^{\circ}$; (c) and (c′) ^{1}H and ^{13}C spectra at $\theta = 180^{\circ}$.

longer in the same quantum state but can be found in one of the two states, $|u\rangle$ or $|d\rangle$, with equal probability.

To be more specific, let us consider a system of N coupled two-level systems (qubits). A cluster of spins ½ is a natural physical implementation of such system. As the two most distinct states, one can choose the ferromagnetic states $|u\rangle = |\uparrow\uparrow\uparrow\uparrow\uparrow\uparrow\rangle$ and $|d\rangle = |\downarrow\downarrow\downarrow\downarrow\downarrow\downarrow\rangle$ with all spins up and down, respectively. These two states have the maximum difference in polarization (magnetization). The off-diagonal part, N-quantum (NQ) coherence, of the cat state density matrix $\rho = 2^{-1}(|u\rangle + |d\rangle)(\langle u| + \langle d|)$ has the operator form (see [2]) $|u\rangle\langle d| + |d\rangle\langle u| = S_1^+ S_2^+ \ldots S_N^+ + S_1^- S_2^- \ldots S_N^-$, where S_i+ and S_i^- are the raising and lowering operators for individual spins. When individual spins are rotated by angles φ_i around their quantization axes, the two product operator terms in the NQ coherence acquire the phases $\pm\Sigma_i\varphi_i$. Therefore, only the sum of the phases is important. This unique feature of the cat state opens a way to interesting applications. First, N times faster rotation of the phase of the cat state, compared to that of an individual spin, is used in high-precision measurements of phases and frequencies (*35*). On the other hand, local rotation of a single spin can produce a global change of the phase for the entire system, which can be then converted into a change of macroscopic observables. This creates a base for amplified quantum detection (*7*, *33*) and state measurement (*8*).

The negative side of these useful properties is high sensitivity of the cat state to phase noise. When interaction with environment produces uncorrelated rotations of individual spins by $\Delta\varphi_i$, the change in the phase of the NQ coherence, $\Delta\varphi$, can be estimated as $\langle\Delta\varphi^2\rangle \approx N\langle\Delta\varphi_i^2\rangle$. This explains why even weak interaction with environment may cause fast decoherence in macroscopic systems. Random phases acquired by the NQ coherences of individual systems average out the off-diagonal part of the cat state density matrix and convert it to the diagonal mixed state. Decoherence can be viewed as a loss of information about the phase of the NQ coherence of an individual system. This also means a loss of reversibility because, in order to dynamically convert a state into some target state, one needs to know the exact starting state. A degree of irreversibility is quantified by the entropy, which changes from zero for the pure cat state to k_B ln 2 for the mixed state.

Different states of the same system have different sensitivity to noise. Some of them are resistant to relaxation and decoherence (*43–46*). The cat state is the most fragile in terms of the decoherence rate, but the damage produced to this state by decoherence is relatively small. In quantum mechanics, density matrix gives the most complete description of a system. This means that no physical measurement can distinguish between the mixed state $\rho = 2^{-1}(|u\rangle\langle u| + |d\rangle\langle d|)$, resulting from averaging out the NQ coherences, and the mixture of systems in one of the two states, $|u\rangle$ or $|d\rangle$. Therefore, the only missing information is which of the two states has been chosen by a system. This information can be stored in only one additional qubit.

Let us consider a combined system of $N + 1$ qubits. The symbols $|\uparrow\rangle$ and $|\downarrow\rangle$ will denote the two states of the additional qubit. It will be called a control qubit because its state will be used to control a change of the state of the N-qubit system. We will start with the system in some superposition of the states $|u\rangle$ and $|d\rangle$ and the control qubit in its ground state $|\uparrow\rangle$:

$$|\Psi\rangle_{\text{in}} = |\uparrow\rangle(a|u\rangle + b|d\rangle), \quad |a|^2 + |b|^2 = 1. \quad [7]$$

By using interaction between the control qubit and the system, one can design a reversible unitary evolution (*8*), which converts the state [7] into the state

$$|\Psi\rangle_{\text{out}} = a|\uparrow\rangle|u\rangle + b|\downarrow\rangle|d\rangle. \quad [8]$$

Decoherence eliminates the $(N+1)$Q coherence in this state and produces the mixed state with the density matrix

$$\rho_{\text{mix}} = aa^*|\uparrow\rangle\langle\uparrow| \otimes |u\rangle\langle u| + bb^*|\downarrow\rangle\langle\downarrow| \otimes |d\rangle\langle d|. \quad [9]$$

In this mixture of two states, information about the state of the N-qubit system (is it $|u\rangle$ or $|d\rangle$) is stored in the state of the control qubit. It is possible to use this information for producing a dynamic evolution, conditioned by the state of the control qubit, which will bring the N-qubit system to a desired pure state, as an example, the *alive* state $|u\rangle$.

Alternatively, the density matrix [9] can be viewed as resulting from projective measurement, where the control qubit is used as a "measuring device." The initial superposition state of the N-qubit system, $a|u\rangle + b|d\rangle$, is collapsed into one of the two definite states $|u\rangle$ or $|d\rangle$, while the remaining uncertainty is compensated by the measurement result, stored in the state of the control qubit.

Creation of the pseodopure state $|\uparrow\rangle|u\rangle$ for our 7-spin system is the first part (step A) of the experimental scheme in Fig. 13. ^{1}H linear-response spectra of the four pseudopure states are shown in Fig. 14. The states $|\uparrow\rangle|d\rangle$, $|\downarrow\rangle|u\rangle$, and $|\downarrow\rangle|d\rangle$ are obtained from the state $|\uparrow\rangle|u\rangle$ by applying "hard" 180° carbon and proton pulses. The left column in Fig. 14 displays the

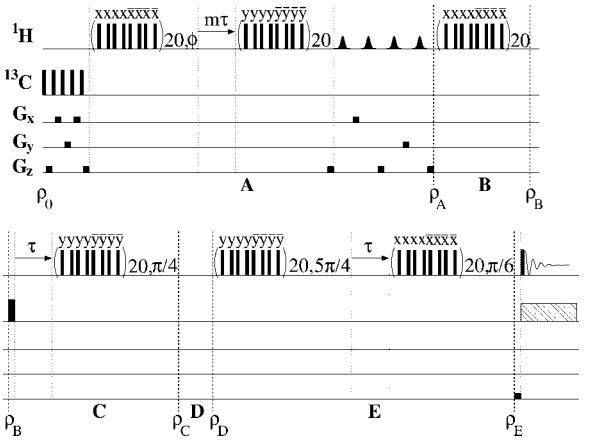

Figure 13 NMR pulse sequence used to resurrect the Schrodinger cat: (Step A) six proton spins and a carbon spin are initialized in the pseudopure state ($m = 0$, 1 and $\tau = 201$ μs); (step B) the proton's cat state is prepared; (step C) the ^{13}C spin is entangled with the proton spins; (step D) decoherence brings the whole system into a mixed state; (step E) the "controlled-not" operation, conditioned on the ^{13}C spin state, creates the target state of the proton subsystem.

spectra with decoupled ^{13}C spin. Each of the decoupled spectra (left column) consists of a single peak. The ^{13}C-coupled spectra for the states $|\uparrow\rangle|u\rangle$ [Fig. 14(b′)] and $|\downarrow\rangle|d\rangle$ [Fig. 14(e′)] have two peaks, and there are one large and two smaller peaks in the spectra for the states $|\uparrow\rangle|d\rangle$ [Fig. 14(c′)] and $|\downarrow\rangle|u\rangle$ [Fig. 14(d′)]. For comparison, the thermal equilibrium spectra are shown in Figs. 14(a,a′).

Step B of the experiment (Fig. 13) creates the six-spin cat state for the proton subsystem and, therefore, the total state becomes that of Eq. [7] (at $a = b = 2^{-1/2}$), which is the starting point of our "resurrection" scheme. The next step C (Fig. 13) is designed to convert the protons' 6-spin cat state of Eq. [7] into the 7-spin cat state of the entire system, described by Eq. [8]. This step includes 90° ^{13}C pulse, ^{13}C–proton evolution delay, and protons MQ evolution period. The ^{13}C-decoupled and ^{13}C-coupled spectra of this 7-spin cat state are shown in Figs. 15(a,a′), respectively.

The variable-length step D is a delay when decoherence takes place and converts the pure state [8] into the mixed state [9]. Before proceeding to the next step, we measured the decay times of the off- diagonal, i.e. the 7Q coherence, and the diagonal elements of the 7-spin cat state density matrix to see how decoherence transforms a superposition state into a mixture. Decays of both the off-diagonal and the diagonal elements of the cat state are well described by single-exponential curves with the average lifetimes of 29 and 490 ms, respectively.

The last step E of the experiment (Fig. 13) implements the "controlled-not" operation: when the state of the control qubit is $|\uparrow\rangle$, it does not change the state of the proton subsystem; when the state of the qubit is $|\downarrow\rangle$, it flips the protons state $|d\rangle$ into the state $|u\rangle$ and vice versa. As a result, a mixture of the two states $|\uparrow\rangle|u\rangle$ and $|\downarrow\rangle|d\rangle$ after step D is converted into a new mixture of the states $|\uparrow\rangle|u\rangle$ and $|\downarrow\rangle|u\rangle$. In both of these states the proton subsystem is in the target *alive* state $|u\rangle$. This is supported by the ^{13}C-decoupled spectra in Figs. 15(c,d) for 100 and 200 ms delays in step D. The spectra are the same as the spectrum of the pseudopure state $|u\rangle$ in Figs. 14(b,d). One can see that even after 200 ms delay time, which is much longer than the 7-spin cat state decoherence time (29 ms) or the protons 6-spin cat state decoherence time (42 ms), the target state $|u\rangle$ is well recovered. At the same time, the ^{13}C spin is found in the mixture of the two states $|\uparrow\rangle$ and $|\downarrow\rangle$, which can be clearly seen in the ^{13}C-coupled spectra in Figs. 15(c′,d′). These spectra are the sums of the spectra for the two pseudopure states $|\uparrow\rangle|u\rangle$ and $|\downarrow\rangle|u\rangle$ in Figs. 14(b′,d′). Therefore, the excess entropy $k_B \ln 2$ produced by decoherence is transferred to the ^{13}C spin. As it was mentioned above, this step resembles a projective measurement, where the ^{13}C spin plays a role of "measuring device."

Our purification scheme resembles an active quantum error-correcting algorithm (*47*). In both cases, additional resources are used to bring the system back to the target pure state after decoherence or errors. Simple quantum error-correcting schemes have been experimentally realized for small quantum systems (*48–50*). Compared with these experiments, demonstrating protection from artificial errors and engineered decoherence effects, our experiment implements a state purification after uncontrollable natural decoherence.

POSSIBLE OUTCOMES OF QUANTUM MEASUREMENT

In this section, we show that NMR experiments using pseudopure spin states can give possible outcomes of projective quantum measurement and probabilities of such outcomes (*51*). For the cluster of six dipolar-coupled nuclear spins of benzene in a liquid-crystalline matrix, a system with the maximum total spin $S = 3$, the results of measuring S_X are presented for the cases when the state of the system is one of the eigenstates of S_Z.

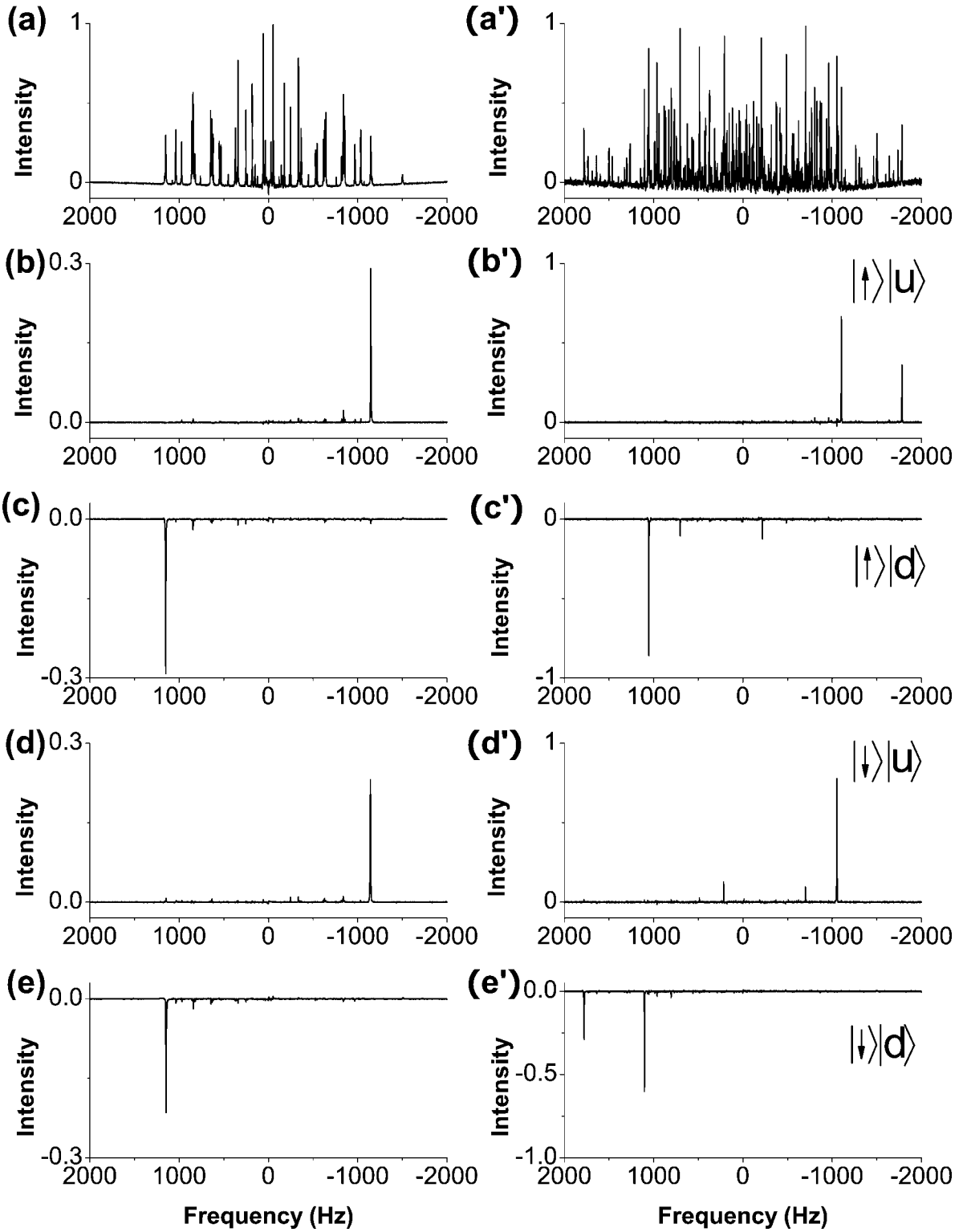

Figure 14 Linear-response ^{1}H NMR spectra at thermal equilibrium (a,a′) and for four pseudo-pure states (b–e and b′–e′). The left column shows ^{13}C-decoupled spectra.

Interesting quantum algorithms, like teleportation (*26*) or factorization of numbers (*29*), in their original formulation, rely on projective measurement and collapse of wave function. Possibility to retrieve the results of projective measurements from NMR experiments enhances capabilities of NMR as an

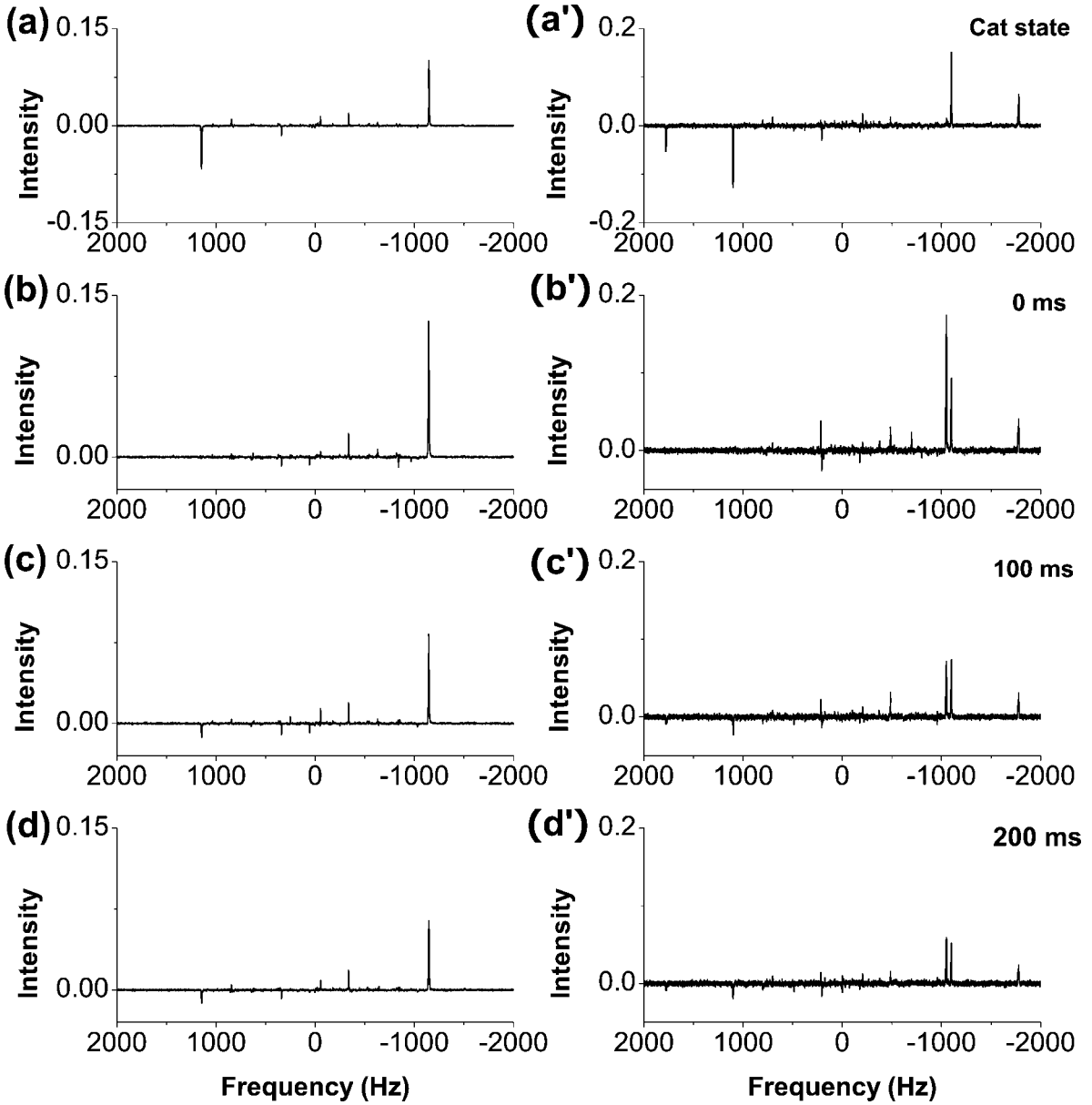

Figure 15 Linear-response ^{1}H NMR spectra for the seven-spin cat state (a,a′), and the restored 6-spin *alive* state $|u\rangle$. The delay times are (b,b′) 0 ms, (c,c′) 100 ms, and (d,d′) 200 ms. The left column shows ^{13}C-decoupled spectra.

inexpensive tool for testing quantum algorithms. The experiment we describe here has been performed on clusters of six dipolar-coupled proton spins of benzene in liquid crystal ZLI-1167 at 25°C using Varian Unity/Inova 500 MHz NMR spectrometer. The spin Hamiltonian is

$$H = -\omega_0 \sum_{k=1}^{6} S_{kS} + \sum_{k=1}^{6} b_{jk} \{ S_{kZ} S_{jZ} - \tfrac{1}{2} S_{kX} S_{jX} - \tfrac{1}{2} S_{kY} S_{jY} \}, \quad [10]$$

where ω_0 is the Larmor frequency, S_{kX}, S_{kY}, and S_{kZ} are the components of kth spin, and b_{jk} are the constants of residual dipole–dipole interaction. J-couplings between the proton spins are small, with the largest one $J_{12}/2\pi = 7.5$ Hz (*19*), and can be neglected.

The eigenfunctions of the system's Hamiltonian [10] are simultaneously eigenfunctions of S_Z, the projection of the total spin on the direction of external magnetic field. We start with one of the eigenfunctions of the Hamiltonian [10] and measure S_X,

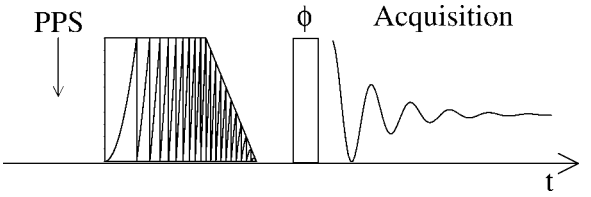

Figure 16 NMR pulse sequence for projective measurement: preparation of pseudopure state is followed by a frequency-sweeping lock pulse of 25 ms duration, initial amplitude $\gamma B_1/2\pi = 19$ kHz, and 20 kHz sweeping during the first 20 ms; a linear-response spectrum is acquired using a small-angle reading pulse.

the x-component of the total spin of the cluster, in the rotating frame. Since S_X does not commute with S_Z, the measurement cannot give a definite value. The amplitudes of probabilities of possible outcomes are projections of the initial state on the eigenstates of S_X. To project the state of the system on the S_X eigenstates, we instantly turn on a strong field along x-axis of the rotating frame, as it is shown on the experimental scheme in Fig. 16. This strong field not only locks the total magnetization (*52*) but also preserves populations of individual eigenstates of S_X corresponding to different values of the magnetic quantum number M_X (transitions changing M_X are forbidden by the energy conservation). Then, the frequency of the RF pulse gradually changes so that the direction of the effective field adiabatically rotates towards z-axis. When the frequency offset becomes much greater than the dipole–dipole interactions in the cluster, the amplitude of the RF pulse is adiabatically decreased to zero. As a result, each of the S_X eigenstates is adiabatically converted into one of the eigenstates of the system's Hamiltonian with the same value of the magnetic quantum number (*53*). Populations of these states, obtained from linear-response NMR spectra, give probabilities of different values of M_X for the initial state.

The Hamiltonian [10] does not commute with S^2. However, its eigenstates with $M_Z = \pm 3$ and $M_Z = \pm 2$ are also the eigenstates of S^2. Two states with all spins up ($M_Z = +3$) or down ($M_Z = -3$) are $S = 3$ states. Twelve states with $M_Z = \pm 2$ are spin waves (*54*). Two states with the wave number $k = 0$ are $S = 3$ states. Ten other spin waves with $k \neq 0$ are $S = 2$ states.

The first experiment starts with the ($S = 3$, $M_Z = 3$) pseudopure state. Linear-response spectrum of this state, shown in Fig. 17(b), has only one peak corresponding to a SQ transition to the ($S = 3$, $M_Z = 2$) state. Since the initial state is an eigenstate of S^2 with $S = 3$, it projects on only seven of the S_X eigenstates, which belong to the $S = 3$ subspace and can be described by a single quantum number M_X ranging from -3 to $+3$. Adiabatic pulse converts each of these seven states into one of the seven high-spin eigenstates of the Hamiltonian [10] with the same magnetic quantum number. The high-spin eigenstates with $M_Z = \pm 3$ and $M_Z = \pm 2$ are $S = 3$ states. The states $M_Z = \pm 1$ and $M_Z = 0$ are, respectively, the states with effective spins $S = 2.78$ and $S = 2.59$, calculated as $S(S + 1) = \langle S^2 \rangle$. At the same time, each of these high-spin states is the state with the lowest energy among the states with the same value of M_Z (*55*). Six SQ transitions between seven high-

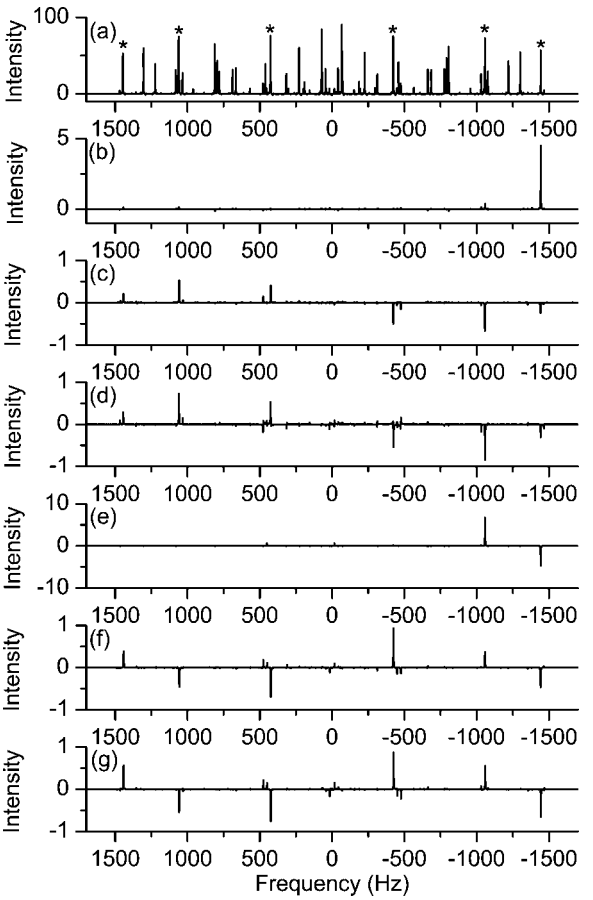

Figure 17 (a) Thermal equilibrium ^{1}H NMR spectrum, the peaks marked by asterisks are the transitions between seven high-spin states; (b) linear-response spectra of the ($S = 3$, $M_Z = 3$) state; (c) linear-response spectrum for the ($S = 3$, $M_Z = 3$) state projected onto S_X by a lock pulse; (d) linear-response spectrum for the ($S = 3$, $M_Z = 3$) state after 90° hard pulse and gradient dephasing; (e) linear-response spectrum of the ($S = 3$, $M_Z = 2$) state; (f) linear-response spectrum for the ($S = 3$, $M_Z = 2$) state projected onto S_X by a lock pulse; (g) linear-response spectrum for the ($S = 3$, $M_Z = 2$) state after 90° hard pulse and gradient dephasing.

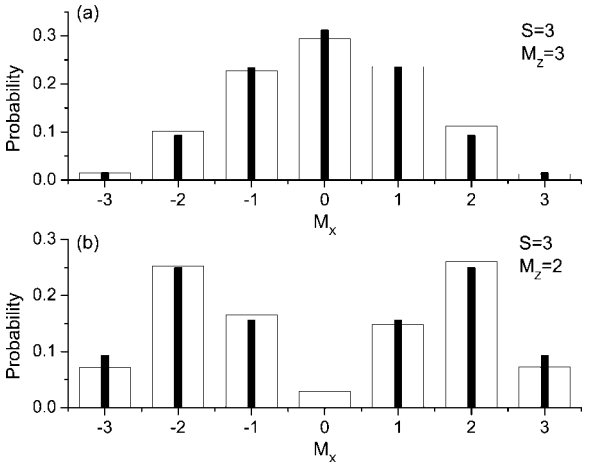

Figure 18 Probabilities of different values of M_X for the initial (a) ($S = 3$, $M_Z = 3$) and (b) ($S = 3$, $M_Z = 2$) states are shown with wide bars; narrow bars are the theoretical values.

spin eigenstates are marked with asterisks in the thermal-equilibrium spectrum in Fig. 17(a). At thermal equilibrium, all differences of populations for pairs of states with $\Delta M_Z = 1$ are equal and, therefore, the intensities of the peaks in Fig. 17(a) are proportional to the transition probabilities (squares of the transition matrix elements).

The result of experiment for the initial ($S = 3$, $M_Z = 3$) state is shown in Fig. 17(c). Analysis of this linear-response spectrum confirms that only seven high-spin eigenstates of the Hamiltonian [10] are populated. Six differences of populations for these seven states are obtained from intensities of six major peaks in Fig. 17(c), normalized by the transition probabilities. The integration constant is obtained from the condition that the sum of populations equals to the population of the pseudopure state in Fig. 17(b). Experimental populations of the seven states, which represent probabilities of seven different outcomes of the M_X measurement are shown in Fig. 18(a). The theoretical probabilities: 1/64, 6/64, 15/64, 20/64, 15/64, 6/64, 1/64 for M_X ranging from -3 to $+3$ are also shown in Fig. 18(a) for comparison. The theoretical value of $\langle S_X^2 \rangle$ for the ($S = 3$, $M_Z = 3$) state is $\langle S_X^2 \rangle = \langle S_Y^2 \rangle = \frac{1}{2}[S(S+1) - M_Z^2] = \frac{3}{2}$. The value calculated with the experimental probability distribution in Fig. 18(a) is $\langle S_X^2 \rangle = 1.57$.

Another way to obtain the results of projective measurement is to rotate eigenfunctions of the measured operator to the measurement basis. This method has been used in experiments with trapped ions (*56*) and photons (*57*). Linear-response spectrum after applying a 90° hard pulse to the ($S = 3$, $M_Z = 3$) state and dephasing with magnetic field gradient is shown in Fig. 17(d). Gradient dephasing has been used before to imitate the effect of projective measurement in NMR (*58*). Although the spectra 17(c) and 17(d) look similar, they are not the same. Since there are no $S = 3$ eigenstates of the system's Hamiltonian with $M_Z = \pm 1$ and $M_Z = 0$, many $M_Z = \pm 1$ and $M_Z = 0$ states become populated in the experiment using 90° pulse, which results in additional small peaks in Fig. 17(d).

The second experiment starts with the pseudopure eigenstate of the Hamiltonian [10] with $S = 3$ and $M_Z = 2$, which was obtained from the ($S = 3$, $M_Z = 3$) state by applying a 180° Gaussian selective pulse of 30-ms duration and maximum amplitude $\gamma B_1/2\pi = 15$ Hz at the frequency of the peak in Fig. 17(b). The linear-response spectrum for this state is shown in Fig. 17(e). It consists of one negative peak, which is the transition to the ($S = 3$, $M_Z = 3$) state, one large positive peak, which is the transition to the high-spin $M_Z = 1$ state, and two small positive peaks, which are the transitions to two other $M_Z = 1$ states (*20*) and are barely seen in Fig. 17(e). For the initial ($S = 3$, $M_Z = 2$) state, experimental populations of the seven states, which represent probabilities of seven different outcomes of the M_X measurement, are shown in Fig. 18(b). The theoretical probabilities: 3/32, 8/32, 5/32, 0, 5/32, 8/32, 3/32 for M_X ranging from -3 to $+3$ are also shown in Fig. 18(b). The theoretical value of $\langle S_X^2 \rangle$ for the state with $S = 3$ $M_Z = 2$ is $\langle S_X^2 \rangle = \langle S_Y^2 \rangle = \frac{1}{2}[S(S+1) - M_Z^2] = 4$. The value calculated with the experimental probability distribution in Fig. 18(b) is $\langle S_X^2 \rangle = 3.66$.

In general terms, the described technique is based on turning on instantly the Hamiltonian representing the measured quantity and then, adiabatically changing it to another Hamiltonian with spectroscopically distinguishable eigenstates.

ADIABATIC TRANSFER OF COHERENCES

Here we demonstrate that quantum coherences can be efficiently transferred using adiabatic energy-level crossing (*55*).

The quantum adiabatic theorem (*53*) tells that, when external parameters change very slowly, a quantum system prepared in an eigenstate of the initial Hamiltonian evolves into one of the eigenstates of the final Hamiltonian if the rates of nonadiabatic transitions between different instantaneous eigenstates are negligible during the evolution (*59*). Population of a quantum state can be transferred to another state by adiabatic energy-level crossing, as

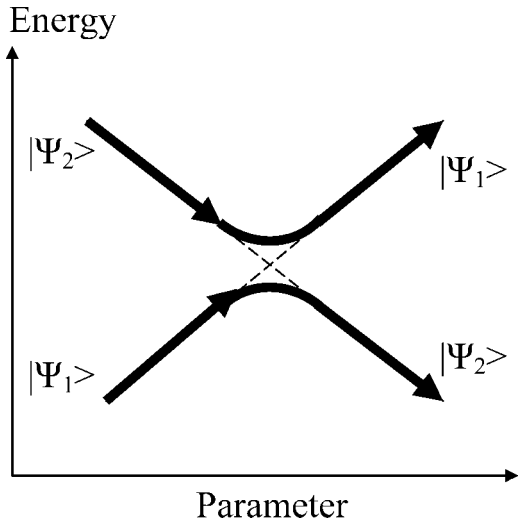

Figure 19 Switching quantum states with adiabatic energy-level crossing.

schematically shown in Fig. 19. It is a well-known phenomenon, extensively studied both theoretically and experimentally for various quantum systems. Adiabaticity, i.e. conservation of entropy, and linearity of quantum mechanics suggest that superpositions of states should not be destroyed by such adiabatic switches. As an example, if a system is prepared in the superposition state $2^{-1/2}(|0\rangle + |1\rangle)$ and then, the population of state $|1\rangle$ is adiabatically transferred into the population of state $|2\rangle$, we would expect that the final state of the system will be the superposition state $2^{-1/2}(|0\rangle + |2\rangle)$.

Adiabatic transfer of superposition states has been studied for small atomic systems (*60*), and recent development of QC attracted some attention to using adiabatic evolution for implementing quantum logic gates (*61*).

According to the quantum adiabatic theorem, the state gains some dynamical phase factor, which is not detectable since the state is an eigenstate at all times. A general quantum state is a superposition of eigenstates, where a relative phase between individual eigenfunctions can be measured. Interesting questions are whether the coherences can be transferred by adiabatic energy-level crossing and what happens to the relative phases. As it is shown below, when populations of the states are adiabatically transferred via multiple energy-level crossings, not only the coherence is transferred but the relative phase between eigenstates can be preserved. The relative phase between two quantum states is observed as a phase of NMR signal in our experiment.

The experiment has been performed with a Varian Unity/Inova 500 MHz NMR spectrometer. The sample contained 6% of benzene dissolved in liquid-crystalline solvent MLC-6815. Under RF irradiation, the Hamiltonian of the proton spins is

$$H = -\omega_0 \sum_{k=1}^{6} S_{kZ} - 2\omega_1 \sum_{k=1}^{6} S_{kX} \cos \omega t + \sum_{k>j>0}^{6} b_{jk}\left(S_{kZ}S_{jZ} - \tfrac{1}{2}S_{kX}S_{jX} - \tfrac{1}{2}S_{kY}S_{jY}\right), \quad [11]$$

where ω_1 and ω are the amplitude and the frequency of the RF field, respectively. In the rotating frame, the Hamiltonian transforms into

$$H_{\text{rot}} = -\Delta\omega_{\text{H}} \sum_{k=1}^{6} S_{kZ} - \omega_1 \sum_{k=1}^{6} S_{kX} + \sum_{k>j>0}^{6} b_{jk}\left(S_{kZ}S_{jZ} - \tfrac{1}{2}S_{kX}S_{jX} - \tfrac{1}{2}S_{kY}S_{jY}\right), \quad [12]$$

where $\Delta\omega_{\text{H}} = (\omega_0 - \omega)$ (*62*, *63*). The adiabatic process has been implemented by slowly sweeping the frequency ω of the RF field. The amplitude ω_1 was sufficiently small to avoid undesired transitions between states.

Figure 20(a) shows the energy spectrum of a cluster of six dipolar-coupled proton spins of benzene as

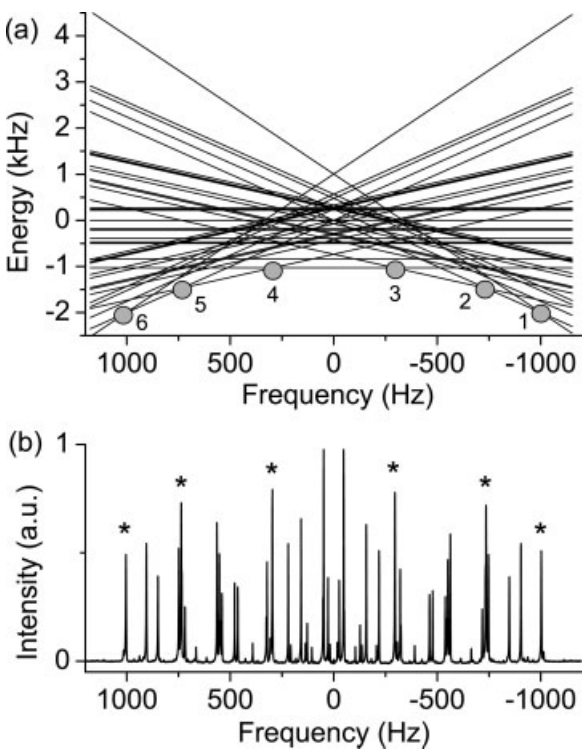

Figure 20 (a) Energy diagram of benzene and (b) thermal equilibrium ^{1}H NMR spectrum.

a function of the offset field $\Delta\omega_H$ in the rotating frame. Each eigenstate is characterized by its magnetic quantum number m, the z component of the total spin angular momentum, which determines the slope of each line in Fig. 20(a). Crossings of pairs of energy levels with $|\Delta m| = 1$ correspond to allowed SQ transitions (*20*). The thermal equilibrium ^{1}H NMR spectrum displayed in Fig. 20(b) shows the frequency positions of allowed SQ transitions. The peak intensities are proportional to the transition probabilities in the high-field approximation ($|\omega_0 \gg b_{jk}|$). The peaks marked by asterisks in Fig. 20(b) were identified as transitions between the states of the subspace of maximum total spin ($S = 3$) by applying RF pulses to the pseudopure ground state with all spins up (*11*). Strong RF pulse conserves the total spin of the system and when applied, as an example, to the pseudopure ground state, excites the transitions only in the $S = 3$ subspace.

Suppose that the system is in one of its eigenstates and the RF field is turned on at some frequency far from any crossings. As the frequency changes, the system stays in the same state until it encounters an energy-level crossing. At the crossing, the RF field removes degeneracy and "switches" the populations of the levels as shown in Fig. 19. If the frequency changes further, one finds that the system stays in the second state. In this way, RF field with sweeping frequency causes a sequence of transitions from one state to another. As an example, suppose that the system is in the ground state and the RF field is turned on at the frequency -1100 Hz [Fig. 20(a)]. If the frequency increases adiabatically, the system stays in the ground state ($m = 3$) until it encounters the crossing 1 in Fig. 20(a) where it switches to the other state, the first excited state with $m = 2$. After that, it stays in this state until it meets the crossing 2 where it switches to the third state with $m = 1$, and so on.

Figure 21 shows the pulse sequence used in the experiment. A single 90° Gaussian pulse P1 excites the initial coherence between the ground ($m = 3$) and the first excited ($m = 2$) states. The duration of this pulse was set to 50 ms to achieve selectivity. This SQ coherence (superposition of $m = 3$ and $m = 2$ states) is directly observable. To discriminate between decoherence and nonadiabatic losses we introduced 80-ms delay, which is equal to the total duration of the two adiabatic pulses used to transfer the coherence. As a result of decoherence, the signal intensity after 80-ms delay decreased to 46% of its initial value. The signal is shown in Fig. 22(a) The pulse P2 (Fig. 21) with adiabatic frequency sweep transfers population of the $m = 2$ state to the state $m = -3$ following the path 2–3–4–5–6 in Fig. 20(a). As a result, a superposition of the state $m = 3$, which has not been affected by the pulse P2, and the state $m = -3$ is created. This 6Q coherence does not produce any NMR signal. We applied the pulse sequence used in (*11*) and independently verified that the 6Q coherence has been excited.

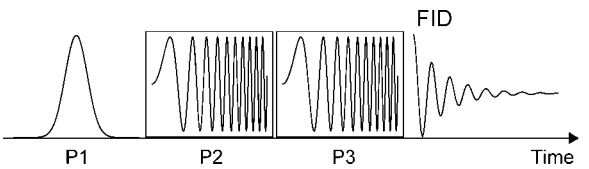

Figure 21 NMR pulse sequence for adiabatic transfer of coherences: 90° Gaussian pulse P1 excites the initial coherence between the ground ($m = 3$) and the first excited ($m = 2$) states. Adiabatic pulses P2 and P3 transfer population of the state with $m = 2$ to the state with $m = -3$ and population of the state with $m = 3$ to the state with $m = -2$, respectively.

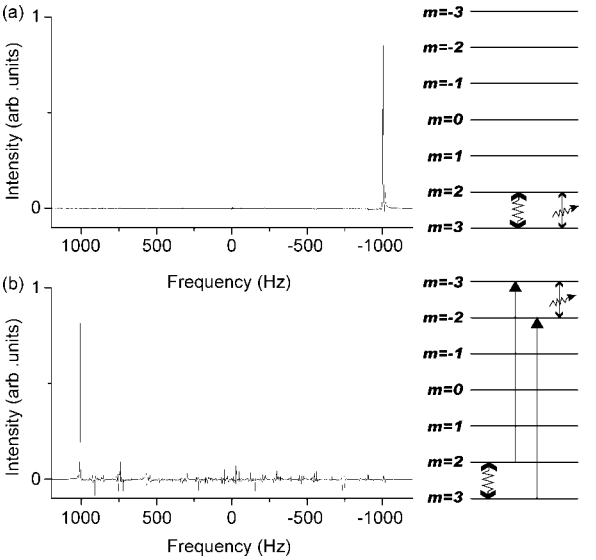

Figure 22 Experimental results: (a) SQ coherence excited by a Gaussian pulse; (b) coherence transferred by two adiabatic demagnetization pulses via ten energy-level crossings.

The pulse P3 (Fig. 21) transfers population of the $m = 3$ state to the state $m = -2$ following the path 1–2–3–4–5 in Fig. 20(a). The resulting state, which contains a SQ coherence between the states $m = -2$ and $m = -3$, produces the NMR signal presented in Fig. 22(b). The intensity of the signal in Fig. 22(b) is 88% of that in Fig. 22(a).

Each of the two adiabatic pulses, P2 and P3, has linear sweeping range of 2200 Hz and 40 ms duration. They are shaped pulses with constant RF

amplitude and 20 K steps of phase increment. The first of them starts at the frequency in the middle between the transitions 1 and 2 in Fig. 20(a), passes the frequencies of the transitions 2, 3, 4, 5, and 6, and ends at the frequency higher than that of the transition 6. The second adiabatic pulse starts at the frequency lower than the transition 1, passes the frequencies of the transitions 1, 2, 3, 4, and 5 and ends at the frequency midway between the transitions 5 and 6 in Fig. 20(a). The transitions caused by the adiabatic pulses are indicated by arrows on the simplified energy diagram in Fig. 22(b).

Recently, adiabatic evolution has been investigated as a potential method for quantum computation (*64–66*). Adiabatic evolution may offer an efficient way of simulating other quantum systems with a quantum computer (*67*). The adiabatic quantum computation has an inherent robustness against unitary control errors, decoherence and relaxation (*65*, *67*). In the experiment described above, we have demonstrated that coherences can be successfully transferred by adiabatic evolution. In the system of six dipolar-coupled nuclear spins, quantum coherence has survived after 10 consecutive adiabatic switches between states.

CONCLUSION

As one could see from the presented examples, clusters of dipolar-coupled nuclear spins, manipulated with NMR techniques, can be used to demonstrate various quantum phenomena. Such systems are, at present, the most complex composite quantum systems, manipulated precisely at the level of individual quantum states. They will be useful in future studies, in implementing new quantum algorithms, and exploring new phenomena in collective quantum dynamics.

ACKNOWLEDGMENTS

The work was supported by the NSF.

REFERENCES

1. Cory DG, Fahmy AF, Havel TF. 1997. Ensemble quantum computing by NMR spectroscopy. Proc Natl Acad Sci USA 94:1634–1639.
2. Gershenfeld N, Chuang IL. 1997. Bulk spin-resonance quantum computation. Science 275:350–356.
3. Jones JA, Mosca M. 1998. Implementation of a quantum algorithm on a nuclear magnetic resonance quantum computer. J Chem Phys 109:1648–1653.
4. Chuang I, Nielsen M. 2000. Quantum Computation and Quantum Information. Cambridge, UK: Cambridge University Press.
5. Somaroo S, Tseng CH, Havel TF, Laflamme R, Cory DG. 1999. Quantum simulations on a quantum computer. Phys Rev Lett 82:5381.
6. Khitrin AK, Fung BM. 2001. NMR simulation of an eight-state quantum system. Phys Rev A 64:032306.
7. Lee J-S, Khitrin AK. 2004. Quantum amplifier: measurement with entangled spins. J Chem Phys 121: 3949–3951.
8. Lee J-S, Khitrin AK. 2005. Experimental demonstration of quantum state expansion in a cluster of dipolar-coupled nuclear spins. Phys Rev Lett 94: 150504.
9. Das R, Bhattacharyya R, Kumar A. 2004. Quantum information processing by NMR using a 5-qubit system formed by dipolar coupled spins in an oriented molecule. J Magn Reson 170:310–321.
10. Khitrin A, Sun H, Fung BM. 2001. Method of multifrequency excitation for creating pseudopure states for NMR quantum computing. Phys Rev A 63: 020301.
11. Lee J-S, Khitrin AK. 2004. Preparation of pseudopure states in a cluster of dipolar-coupled spins using multiple-quantum dynamics. Phys Rev A 70: 022330.
12. Vandersypen LMK, Steffen M, Breyta G, Yannoni CS, Sherwood MH, Chuang IL. 2001. Experimental realization of Shor's quantum factoring algorithm using nuclear magnetic resonance. Nature 414:883–887.
13. Negrevergne C, Mahesh TS, Ryan CA, Ditty M, Cyr-Racine F, Power W, et al. 2006. Benchmarking quantum control methods on a 12-qubit system. Phys Rev Lett 96:170501.
14. Knill E, Laflamme R, Martinez R, Tseng C-H. 2000. An algorithmic benchmark for quantum information processing. Nature 404:368–370.
15. Baum J, Munowitz M, Garroway AN, Pines A. 1985. Multiple-quantum dynamics in solid state NMR. J Chem Phys 83:2015–2025.
16. Suter D, Liu SB, Baum J, Pines A. 1987. Multiple quantum NMR excitation with a one-quantum Hamiltonian. Chem Phys 114:103–109.
17. Warren WS, Weitekamp DP, Pines A. 1980. Theory of selective excitation of multiple-quantum transitions. J Chem Phys 73:2084–2099.
18. Slichter CP. 1996. Principles of Magnetic Resonance. New York: Springer-Verlag.
19. Khitrin AK, Fung BM. 1999. Proton polarization transfer in a ring system. J Chem Phys 111:7480–7485.
20. Saupe A. 1965. Das Protenenresonanzspektrum von orientiertem Benzol in nematisch-kristallinflüssiger Lösung. Z Naturforschg 20a:572–580.
21. Warren WS. 1997. The usefulness of NMR quantum computing. Science 277:1688–1690.

22. Lee J-S, Khitrin AK. 2005. Pseudopure state of a twelve-spin system. J Chem Phys 122:041101.
23. Provotorov BN. 1961. Magnetic-resonance saturation in crystals. Zh Eksperim i Teor Fiz 41:1582–1591.
24. Lee J-S, Khitrin AK. 2005. Twelve-spin "Schrödinger cat". Appl Phys Lett 87:204109.
25. Laloë F. 2001. Do we really understand quantum mechanics? Strange correlations, paradoxes, and theorems. Am J Phys 69:655–701.
26. Bennett CH, Brassard G, Crépeau C, Jozsa R, Peres A, Wootters WK. 1993. Teleporting an unknown quantum state via dual classical and Einstein–Podolsky–Rosen channels. Phys Rev Lett 70:1895–1899.
27. Bennett CH, Brassard G. 1984. Quantum cryptography: public key distribution and coin tossing. In: Proceedings of IEEE International Conference on Computers, Systems and Signal Processing. Bangalore: IEEE. p 175.
28. Bennett CH, Bessette F, Brassard G, Salvail L, Smolin J. 1992. Experimental quantum cryptography. J Cryptol 5:3–28.
29. Shor P. 1994. Algorithms for quantum computation: discrete logarithms and factoring. In: Proceedings of 35th Annual Symposium on the Foundations of Computer Science. Los Alamitos, CA: IEEE Computer Society. p 124.
30. Grover LK. 1997. Quantum mechanics helps in searching for a needle in a haystack. Phys Rev Lett 79:325–328.
31. Ramanathan C, Cho H, Cappellaro P, Boutis GS, Cory DG. 2003. Encoding multiple quantum coherences in non-commuting bases. Chem Phys Lett 369:311–317.
32. Lorenz EN. 1972. Predictability: does the flap of a butterfly's wings in Brazil set off a tornado in Texas? Presented at The 139th meeting of the American Association for the Advancement of Science, Washington, DC.
33. Cappellaro P, Emerson J, Boulant N, Ramanathan C, Lloyd S, Cory DG. 2005. Entanglement assisted metrology. Phys Rev Lett 94:020502.
34. Bennett AE, Rienstra CM, Auger M, Lakshmi KV, Griffin RG. 1995. Heteronuclear decoupling in rotating solids. J Chem Phys 103:6951–6958.
35. Leibfried D, Barrett MD, Schaetz T, Britton J, Chiaverini J, Itano WM, et al. 2004. Toward Heisenberg-limited spectroscopy with multiparticle entangled states. Science 304:1476–1478.
36. Bradbury R. 1952. A sound of thunder. In: The Golden Apples of the Sun. New York: Double Play.
37. Paz JP, Zurek WH. 2002. Environment-induced decoherence and the transition from quantum to classical. In: Heiss D, editor. Fundamentals of Quantum Information: Quantum Computation, Communication, Decoherence and All That. Berlin: Springer. p 77–148.
38. Joos E. 2000. Elements of environmental decoherence. In: Blanchard Ph, Giulini D, Joos E, Kiefer C, Stamatescu I-O, editors. Decoherence: Theoretical, Experimental, and Conceptual Problems. Berlin: Springer. p 1–17.
39. Leggett AJ. 2005. The quantum measurement problem. Science 307:871–872.
40. Poulin D. 2005. Macroscopic observables. Phys Rev A 71:022102.
41. Lee J-S, Khitrin AK. 2005. Stimulated wave of polarization in a one-dimensional Ising chain. Phys Rev A 71:062338.
42. Lee J-S, Khitrin AK. 2006. Resurrection of Schrödinger cat. New J Phys 8:144.
43. Carravetta M, Johannessen OG, Levitt MH. 2004. Beyond the T-1 limit: singlet nuclear spin states in low magnetic fields. Phys Rev Lett 92: 153003.
44. Lidar DA, Chuang IL, Whaley KB. 1998. Decoherence-free subspaces for quantum computation. Phys Rev Lett 81:2594–2597.
45. Knill E, Laflamme R, Viola L. 2000. Theory of quantum error correction for general noise. Phys Rev Lett 84:2525–2528.
46. Kribs D, Laflamme R, Poulin D. 2005. Unified and generalized approach to quantum error correction. Phys Rev Lett 94:180501.
47. Shor PW. 1995. Scheme for reducing decoherence in quantum computer memory. Phys Rev A 52:R2493–R2496.
48. Cory DG, Price MD, Maas W, Knill E, Laflamme R, Zurek WH, et al. 1998. Experimental quantum error correction. Phys Rev Lett 81:2152–2155.
49. Knill E, Laflamme R, Martinez R, Negrevergne C. 2001. Benchmarking quantum computers: the five-qubit error correcting code. Phys Rev Lett 86:5811–5814.
50. Chiaverini J, Leibfried D, Schaetz T, Barrett MD, Blakestad RB, Britton J, et al. 2004. Realization of quantum error correction. Nature 432:602–605.
51. Lee J-S, Khitrin AK. 2006. Projective measurement in nuclear magnetic resonance. Appl Phys Lett 89:074105.
52. Levitt MH. 2001. Spin Dynamics. Chichester: John Wiley & Sons. p 551.
53. Messiah A. Quantum Mechanics. New York: Wiley. p 744.
54. Feldman EB, Khitrin AK. 1990. Spin-wave theory of NMR in solids at low-temperatures. Zh Eksp Teor Fiz (JETP) 98:967–977.
55. Lee J-S, Cardwell KE, Khitrin AK. 2005. Adiabatic transfer of coherences in a cluster of coupled nuclear spins. Phys Rev A 72:064101.
56. Haljan PC, Lee PJ, Brickman K-A, Acton M, Deslauriers L, Monroe C. 2005. Entanglement of trapped-ion clock states. Phys Rev A 72:062316.
57. Resch KJ, Walther P, Zeilinger A. 2005. Full characterization of a three-photon Greenberger–Horne– Zeilinger state using quantum state tomography. Phys Rev Lett 94:070402.
58. Xiao L, Jones JA. 2006. NMR analogues of the quantum Zeno effect. Phys Lett A 359:424–427.

59. Kato T. 1950. On the adiabatic theorem of quantum mechanics. J Phys Soc Jpn 5:435–439.
60. Parkins AS, Marte P, Zoller P, Kimble HJ. 1993. Synthesis of arbitrary quantum states via adiabatic transfer of Zeeman coherence. Phys Rev Lett 71: 3095–3098.
61. Goto H, Ichimura K. 2004. Multiqubit controlled unitary gate by adiabatic passage with an optical cavity. Phys Rev A 70:012305.
62. Ernst RR, Bodenhausen G, Wokaun A. 1987. Principles of Nuclear Magnetic Resonance in One and Two Dimensions. Oxford, UK: Clarendon Press.
63. Abragam A. 1961. Principles of Nuclear Magnetism. Oxford, UK: Clarendo.
64. Farhi E, Goldstone J, Gutmann S, Lapan J, Lundgren A, Preda D. 2001. A quantum adiabatic evolution algorithm applied to random instances of an NP-complete problem. Science 292:472–475.
65. Childs AM, Farhi E, Preskill J. 2001. Robustness of adiabatic quantum computation. Phys Rev A 65: 012322.
66. Steffen M, van Dam W, Hogg T, Breyta G, Chuang I. 2003. Experimental implementation of an adiabatic quantum optimization algorithm. Phys Rev Lett 90:067903.
67. Murg V, Cirac JI. 2004. Adiabatic time evolution in spin systems. Phys Rev A 69:042320.

BIOGRAPHIES

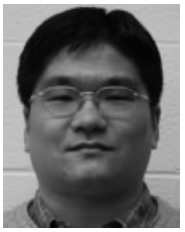

Jae-Seung Lee received his Ph.D. in physics from the Korea Advanced Institute of Science and Technology in 2003 under the guidance of Soonchil Lee. Since 2003 he has been working as a postdoctoral fellow in the group of Anatoly Khitrin at Kent State University. His major research interest is the development of engineered quantum dynamics and their implementation with NMR.

Anatoly Khitrin is a graduate of Moscow Institute of Physics and Technology. In the Institute of Chemical Physics in Chernogolovka, Russia, he worked with Boris Provotorov (1978–1989) on theory of magnetic resonance and spin dynamics. In 1999 he moved to the University of Oklahoma and learned from Bing Fung how to do NMR experiments. Since 2002 Dr. Khitrin is an associate professor at Kent State University in the USA.